

Dynamic Flows on Curved Space Generated by Labeled Data

Xinru Hua¹, Truyen Nguyen², Tam Le³ and Jose Blanchet¹, Viet Anh Nguyen⁴

¹ Stanford University

²The University of Akron

³The Institute of Statistical Mathematics / RIKEN AIP

⁴Chinese University of Hong Kong

Abstract

The scarcity of labeled data is a long-standing challenge for many machine learning tasks. We propose our gradient flow method to leverage the existing dataset (i.e., source) to generate new samples that are close to the dataset of interest (i.e., target). We lift both datasets to the space of probability distributions on the feature-Gaussian manifold, and then develop a gradient flow method that minimizes the maximum mean discrepancy loss. To perform the gradient flow of distributions on the curved feature-Gaussian space, we unravel the Riemannian structure of the space and compute explicitly the Riemannian gradient of the loss function induced by the optimal transport metric. For practical applications, we also propose a discretized flow, and provide conditional results guaranteeing the global convergence of the flow to the optimum. We illustrate the results of our proposed gradient flow method on several real-world datasets and show our method can improve the accuracy of classification models in transfer learning settings.

1 Introduction

A major challenge in many data science applications is the scarcity of labeled data. Data augmentation methods have been studied in the literature; see for example, the noise injection methods [Moreno-Barea *et al.*, 2018], generative models [Yi *et al.*, 2019], and [Shorten and Khoshgoftaar, 2019] for a survey. We consider a setting where one domain has only a few labeled samples for each class, so we cannot train a well-performing classifier with the available data. To alleviate the data scarcity problem in this setting, we propose to enrich the target dataset by generating additional labeled samples. Using generative models is not possible in our setting because they usually require more than a few samples for each class to learn and generate high-quality new samples [Gao *et al.*, 2018]. In our work, we choose a source dataset with extensive labeled data and then flow the labeled data to the target dataset. Precisely, we introduce a novel data augmentation methodology based on a gradient flow approach that minimizes the maximum mean discrepancy (MMD) distance between the target and the augmented data. Therefore, when minimizing the MMD

distance, we are able to obtain an efficient scheme which generates additional labeled data from the target distribution. Our scheme is model-independent and can be applied to any datasets regardless of the number of classes or dimensionality.

Mathematically, we consider a feature space $\mathcal{X} = \mathbb{R}^m$ and a *categorical* label space \mathcal{Y} . We have a source domain dataset consisting of N samples $(x_i, y_i) \in \mathcal{X} \times \mathcal{Y}$ for $i = 1, \dots, N$, and a target domain dataset of M samples $(\bar{x}_j, \bar{y}_j) \in \mathcal{X} \times \mathcal{Y}$ for $j = 1, \dots, M$ ($M \ll N$). The ultimate goal of this paper is to generate new samples in the target domain, and we aim to generate new samples whose distribution is as close as possible to the distribution that governs the target domain.

We here introduce a gradient flow method [Arbel *et al.*, 2019; Mroueh *et al.*, 2019] to synthesize new, unseen data samples. Gradient flow is a continuous flow along the path where a considered loss function decreases its value. Because we have extensive source domain samples, it is possible to flow each source sample towards the target data while minimizing the loss function. The terminal product of the flow will be new samples that can sufficiently approximate the distribution of the target domain. Thus, gradient flow is an approach to synthesize new target domain samples, and is a complement to data augmentation methods, like adding random noise.

Unfortunately, formulating a gradient flow algorithm for labeled data with categorical set \mathcal{Y} is problematic. Indeed, there is no clear metric structure on \mathcal{Y} in order to define the topological neighborhood, this in turn leads to the difficulty of forming the gradients with respect to the categorical component. To overcome this difficulty, we lift each individual label to a richer structure. For example, a label such as “0” is replaced by a mean vector and a covariance matrix based on the whole distribution of the information associated to this particular label. Then it will be much more natural to apply gradient flow algorithms in the space of the lifted representation. A gradient flow on the dataset space with this idea was recently proposed in [Alvarez-Melis and Fusi, 2021] by leveraging a new notion of distance between datasets in [Alvarez-Melis and Fusi, 2020; Courty *et al.*, 2017; Damodaran *et al.*, 2018]. The main idea behind this approach is to reparametrize the categorical space \mathcal{Y} using the conditional distribution of the features, which is assumed to be Gaussian, and then construct a gradient flow on the feature-Gaussian space. Nevertheless, the theoretical analysis in [Alvarez-Melis and Fusi, 2021] focuses solely on the gradients with respect to the feature with no treatment of

the flow with respect to the Gaussian component. In fact, the space of Gaussian distributions is not a (flat) vector space, and extracting gradient information depends on the choice of the metric imposed on this Gaussian space. On the other hand, our method computes the full gradient with respect to the Gaussian component (the mean and covariance matrix component that correspond to the label component).

Our gradient flows minimize the MMD loss function, thus it belongs to the family of MMD gradient flows that was pioneered in [Mroueh *et al.*, 2019; Arbel *et al.*, 2019], and further extended in [Mroueh and Nguyen, 2021]. The MMD function compares two distributions via their kernel mean embeddings on a *flat* reproducing kernel Hilbert space (RKHS). In contrast to the Kullback-Leibler divergence flow, the MMD flow can employ a sample approximation for the target distribution [Liu, 2017]. Further, the squared MMD possesses unbiased sample gradients [Bińkowski *et al.*, 2018; Bellemare *et al.*, 2017]. However, existing literature on MMD flows focus on distributions on flat Euclidean spaces. The flow developed in our paper here is for distributions on a *curved* Riemannian feature-Gaussian space. Moreover, our approach is distinctive from the flow in [Alvarez-Melis and Fusi, 2021] because we impose a specific metric on the Gaussian component, and we compute explicitly the Riemannian gradient of the MMD loss function with respect to this metric to formulate our flow. Table 1 compares our work with two recent papers on gradient flow in theory and numerical experiments.

Recently, generative models [Rezende *et al.*, 2016; Wang *et al.*, 2021] are successful in generating image samples from given distributions. The most important difference with our method is that generative models learn a prior distribution from massive data that are similar to the target data and generate new target samples conditioning on the prior distribution [Wang *et al.*, 2020; Gao *et al.*, 2018]. Comparatively, our algorithm can transfer between two non-similar and non-related distributions, for example, from random Gaussian noise to MNIST in Supplementary B.11. Another benefit of our method is that we provide conditions for global convergence of our algorithms in Section 4, whereas generative models or more specific, generative adversarial networks (GANs), currently do not guarantee global convergence [Wiatrak *et al.*, 2019].

The application of our gradient flow is few-shot transfer learning, where we want to train classifiers with limited labeled data in the target domain. The numerical experiments in Section 5 demonstrate that our gradient flows can effectively augment the target data, and thus can significantly boost the accuracy in the classification task in the few-shot learning setting. Moreover, we run experiments on Tiny ImageNet datasets to highlight that our algorithm is scalable to higher-dimensional image data, that is higher than recent gradient flow works [Alvarez-Melis and Fusi, 2021; Fan and Alvarez-Melis, 2022]. We also compare our method with [Alvarez-Melis and Fusi, 2021], mixup method [Zhang *et al.*, 2017], and traditional data augmentation methods. Results in Supplementary B.8–B.10 show that our method improves the accuracy in transfer learning more than these methods.

Some related works study nonparametric gradient flows using the 2-Wasserstein distance between distributions [Ambrosio *et al.*, 2008; Jordan *et al.*, 1998; Otto, 2001; Villani, 2008;

Santambrogio, 2015; Santambrogio, 2017; Frogner and Poggio, 2020], but only for distributions on Euclidean spaces and a different distance. Nonparametric gradient flows with other metrics include Sliced-Wasserstein Descent [Liutkus *et al.*, 2019], Stein Descent [Liu, 2017; Liu and Wang, 2016], and Sobolev Descent [Mroueh *et al.*, 2019]. However, they also only consider distributions on Euclidean spaces. In particular, [Liu, 2017] introduce Riemannian structures for the Stein geometry on flat spaces, while ours is for an optimal transport metric on a curved space. Parametric flows for training GANs are studied in [Chizat and Bach, 2018; Chen and Li, 2018; Arbel *et al.*, 2020; Mroueh and Nguyen, 2021].

Contributions. We study a gradient flow approach to synthesize new labeled samples related to the target domain. To construct this flow, we consider the space of probability distributions on the feature-Gaussian manifold, and we metrize this space with an optimal transport distance. We summarize the contributions of this paper as follows.

- We study in details the Riemannian structure of the feature-Gaussian manifold in Section 3, as well as the Riemannian structure of the space of probability measures supported on this manifold in Supplementary A.1.
- We consider a gradient flow that minimizes the squared MMD loss function to the target distribution. We describe explicitly the (Riemannian) gradient of the squared MMD in Lemma 5, and we provide a partial differential equation describing the evolution of the gradient flow that follows the (Riemannian) steepest descent direction.
- We propose two discretized schemes to approximate the continuous gradient flow equation in Section 4.1 and 4.2. We provide conditions guaranteeing the global convergence of our gradient flows to the optimum in both schemes.
- In Section 5, we demonstrate numerical results with our method on real-world image datasets. We show that our method can generate high-fidelity images and improve the classification accuracy in transfer learning settings.

Notations. We use \mathbb{S}^n to denote the set of $n \times n$ real and symmetric matrices, and $\mathbb{S}_{++}^n \subset \mathbb{S}^n$ consists of all positive definite matrices. For $A \in \mathbb{S}^n$, $\text{tr}(A) := \sum_i A_{ii}$. We use $\langle \cdot, \cdot \rangle$ and $\| \cdot \|_2$ to denote the standard inner product and norm on Euclidean spaces. Let $\mathcal{P}(X)$ be the collection of all probability distributions with finite second moment on metric space X . If $\varphi : X \rightarrow Y$ is a Borel map and $\nu \in \mathcal{P}(X)$, then the push-forward $\varphi_{\#}\nu$ is the distribution on Y given by $\varphi_{\#}\nu(E) = \nu(\varphi^{-1}(E))$ for all Borel sets $E \subset Y$. For a function f of the continuous time variable t , f_t denotes the value of f at t while $\partial_t f$ denotes the standard derivative of f w.r.t. t . Also, δ_z denotes the Dirac delta measure at z .

All proofs are provided in the Supplementary material.

2 Labeled Data Synthesis via Gradient Flows of Lifted Distributions

In this section, we describe our approach to synthesize target domain samples using gradient flows. A holistic view of our method is presented in Fig. 1.

In the first step, we would need to lift the feature-label space $\mathcal{X} \times \mathcal{Y}$ to a higher dimensional space where a met-

Paper	Dataset	On curved Riemannian space	Gradient has mean and covariance component
[Alvarez-Melis and Fusi, 2021]	synthetic, *NIST, and CIFAR10	✗	✗
[Arbel <i>et al.</i> , 2019]	synthetic	✗	✗
Ours	synthetic, *NIST, and TinyImageNet	✓	✓

Table 1: To the best of our knowledge, we provide the *first* results on the full gradient of the features and lifted labels on a curved Riemannian space. We also conduct numerical experiments on the highest-dimension real-world datasets.

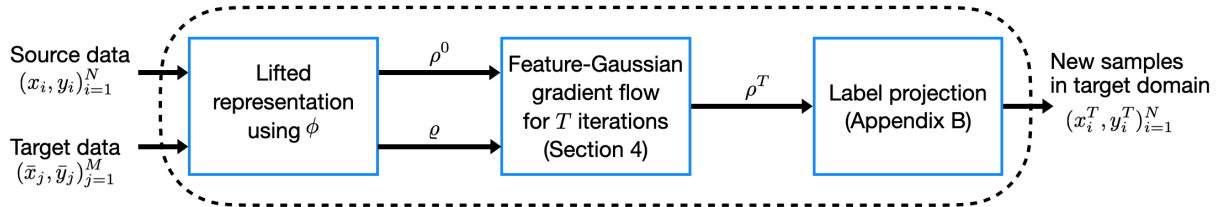


Figure 1: Schematic view of our approach: The source and target datasets are first lifted to distributions ρ^0 and ϱ on the feature-Gaussian space (left box). We then run a gradient flow for T iterations to get a terminal distribution ρ^T (middle). Atoms of ρ^T are projected to get labeled target samples (right).

ric can be defined. Consider momentarily the source data samples $(x_i, y_i)_{i=1}^N$. Notice that this data can be represented as an empirical distribution ν on $\mathcal{X} \times \mathcal{Y}$. More precisely, we have $\nu = N^{-1} \sum_{i=1}^N \delta_{(x_i, y_i)}$. As \mathcal{Y} is discrete, the law of conditional probabilities allows us to dis-integrate ν into the conditional distributions ν_y of $X|Y = y$ satisfying $\nu(E \times F) = \int_F \nu_y(E) \nu^2(dy)$ for every $E \subset \mathcal{X}$ and $F \subset \mathcal{Y}$, where $\nu^2 := N^{-1} \sum_{i=1}^N \delta_{y_i}$ is the second marginal of ν [Ambrosio *et al.*, 2008, Theorem 5.3.1]. The lifting procedure is obtained by employing a pre-determined mapping $\phi : \mathcal{X} \rightarrow \mathbb{R}^n$, and any categorical value $y \in \mathcal{Y}$ can now be represented as an n -dimensional distribution $\phi_{\#} \nu_y$. Using this lifting, any source sample $(x_i, y_i) \in \mathcal{X} \times \mathcal{Y}$ is lifted to a point $(x_i, \phi_{\#} \nu_{y_i}) \in \mathcal{X} \times \mathcal{P}(\mathbb{R}^n)$ and the source dataset is representable as an empirical distribution of the form $N^{-1} \sum_{i=1}^N \delta_{(x_i, \phi_{\#} \nu_{y_i})}$.

The lifted representation of a categorical value $y \in \mathcal{Y}$ as an n -dimensional distribution $\phi_{\#} \nu_y \in \mathcal{P}(\mathbb{R}^n)$ is advantageous because $\mathcal{P}(\mathbb{R}^n)$ is metrizable, for example, using the 2-Wasserstein distance. The downside is that $\mathcal{P}(\mathbb{R}^n)$ is infinite dimensional, and encoding the datasets in this lifted representation is not efficient. To resolve this issue, we assume that $\phi_{\#} \nu_y$ is Gaussian for all $y \in \mathcal{Y}$, and thus any distribution $\phi_{\#} \nu_y$ can be characterized by the mean vector $\mu_y \in \mathbb{R}^n$ and covariance matrix $\Sigma_y \in \mathbb{S}_{++}^n$ defined as $\mu_y = \int_{\mathcal{X}} \phi(x) \nu_y(dx)$ and $\Sigma_y = \int_{\mathcal{X}} [\phi(x) - \mu_y][\phi(x) - \mu_y]^\top \nu_y(dx)$ for all $y \in \mathcal{Y}$, where $^\top$ denotes the transposition of a vector. In real-world settings, the conditional moments of $\phi(X)|Y$ are sufficiently different for $y \neq y'$, and thus the representations using (μ_y, Σ_y) will unlikely lead to any loss of label information. With this lifting, the source data thus can be represented as an empirical distribution ρ^0 on $\mathbb{R}^m \times \mathbb{R}^n \times \mathbb{S}_{++}^n$ via $\rho^0 = N^{-1} \sum_{i=1}^N \delta_{(x_i, \mu_{y_i}, \Sigma_{y_i})}$. By an analogous construction to compute $\bar{\mu}_y$ and $\bar{\Sigma}_y$ using the target data, the target domain data $(\bar{x}_j, \bar{y}_j)_{j=1}^M$ can be represented as another empiri-

cal distribution $\varrho = M^{-1} \sum_{j=1}^M \delta_{(\bar{x}_j, \bar{\mu}_{\bar{y}_j}, \bar{\Sigma}_{\bar{y}_j})}$. Let us denote the shorthand $\mathcal{Z} = \mathbb{R}^m \times \mathbb{R}^n \times \mathbb{S}_{++}^n$, then ρ^0 and ϱ are both probability measures on \mathcal{Z} . We refer to ρ^0 and ϱ as the feature-Gaussian representations of the source and target datasets.

We now consider the gradient flow associated with the optimization problem

$$\min_{\rho \in \mathcal{P}(\mathcal{Z})} \left\{ \mathcal{F}(\rho) := \frac{1}{2} \text{MMD}(\rho, \varrho)^2 \right\}$$

under the initialization $\rho = \rho^0$. The objective function $\mathcal{F}(\rho)$ quantifies how far an incumbent solution ρ is from the target distribution ϱ , measured using the MMD distance. In Sections 3 and 4, we will provide the necessary ingredients to construct this flow.

Suppose that after T iterations of the discretized gradient flow algorithm, we obtain a distribution $\rho^T \in \mathcal{P}(\mathcal{Z})$ that is sufficiently close to ϱ , i.e., $\mathcal{F}(\rho^T)$ is close to zero. Then we can recover new target labels by projecting the samples of the distribution ρ^T to the locations on $\mathcal{X} \times \mathcal{Y}$. This projection can be computed efficiently by solving a linear optimization problem, as discussed in Supplementary B.3.

Remark 1 (Reduction of dimensions). *If $m = n$ and ϕ is the identity map, then our lifting procedure coincides with that proposed in [Alvarez-Melis and Fusi, 2020]. However, a large n is redundant, especially when the cardinality of \mathcal{Y} is low. If $n \ll m$, then ϕ offers significant reduction in the number of dimensions, and will speed up the gradient flow algorithms.*

Remark 2 (Generalization to elliptical distributions). *Our framework can be extended to the symmetric elliptical distributions because the Bures distance for elliptical distributions admits the same closed-form as for the Gaussian distributions [Gelbrich, 1990]. In this paper, we use ϕ as the t-SNE embedding. According to [van der Maaten and Hinton, 2008], t-SNE's low-dimensional embedded space forms a Student-t distribution, which is an elliptical distribution.*

3 Riemannian Geometry of \mathcal{Z} and $\mathcal{P}(\mathcal{Z})$

If we opt to measure the distance between two Gaussian distributions using the 2-Wasserstein metric, then this choice would induce a natural distance d on the space $\mathcal{Z} = \mathbb{R}^m \times \mathbb{R}^n \times \mathbb{S}_{++}^n$ prescribed as

$$d((x_1, \mu_1, \Sigma_1), (x_2, \mu_2, \Sigma_2)) := [\|x_1 - x_2\|_2^2 + \|\mu_1 - \mu_2\|_2^2 + \mathbb{B}(\Sigma_1, \Sigma_2)^2]^{\frac{1}{2}}, \quad (3.1)$$

where \mathbb{B} is the Bures metric on \mathbb{S}_{++}^n given by $\mathbb{B}(\Sigma_1, \Sigma_2) := [\text{tr}(\Sigma_1 + \Sigma_2 - 2[\Sigma_1^{\frac{1}{2}}\Sigma_2\Sigma_1^{\frac{1}{2}}])^{\frac{1}{2}}]^{\frac{1}{2}}$.

As \mathbb{B} is a metric on \mathbb{S}_{++}^n [Bhatia *et al.*, 2019, p.167], d is hence a product metric on \mathcal{Z} . In this section, first, we study the non-Euclidean geometry of \mathcal{Z} under the ground metric d . Second, we investigate the Riemannian structure on $\mathcal{P}(\mathcal{Z})$, the space of all distributions supported on \mathcal{Z} and with finite second moment, that is induced by the optimal transport distance. These Riemannian structures are required to define the Riemannian gradients of any loss functionals on $\mathcal{P}(\mathcal{Z})$, and will remain important in our development of the gradient flow for the squared MMD.

The space \mathcal{Z} is not a linear vector space. In this section, we reveal the Riemannian structure on \mathcal{Z} associated to the ground metric d . As we shall see, \mathcal{Z} is a curved space as its geodesics are not straight lines and involve solutions to the Lyapunov equation. For any positive definite matrix $\Sigma \in \mathbb{S}_{++}^n$ and any symmetric matrix $V \in \mathbb{S}^n$, the Lyapunov equation

$$H\Sigma + \Sigma H = V \quad (3.2)$$

has a unique solution $H \in \mathbb{S}^n$ [Bhatia, 1997, Theorem VII.2.1]. Let $L_\Sigma[V]$ denote this unique solution H .

The space \mathbb{S}_{++}^n is a Riemannian manifold with the Bures metric \mathbb{B} as the associated distance function, see [Takatsu, 2011, Proposition A]. Since \mathcal{Z} is the product of two Euclidean spaces and \mathbb{S}_{++}^n , this gives rise to the following geometric structure for \mathcal{Z} .

Proposition 3 (Geometry of \mathcal{Z}). *The space \mathcal{Z} is a Riemannian manifold: at each point $z = (x, \mu, \Sigma) \in \mathcal{Z}$, the tangent space is $T_z\mathcal{Z} = \mathbb{R}^m \times \mathbb{R}^n \times \mathbb{S}^n$ and the Riemannian metric is*

$$\langle (w_1, v_1, V_1), (w_2, v_2, V_2) \rangle_z := \langle w_1, w_2 \rangle + \langle v_1, v_2 \rangle + \langle V_1, V_2 \rangle_\Sigma \quad (3.3)$$

for two tangent vectors (w_1, v_1, V_1) and (w_2, v_2, V_2) in $\mathbb{R}^m \times \mathbb{R}^n \times \mathbb{S}^n$, where $\langle V_1, V_2 \rangle_\Sigma := \text{tr}(L_\Sigma[V_1]\Sigma L_\Sigma[V_2])$. Moreover, the distance function corresponding to this Riemannian metric coincides with the distance d given by (3.1).

As \mathcal{Z} is a product Riemannian manifold, any geodesic in \mathcal{Z} is of the form (θ, γ, Γ) with θ, γ being the Euclidean geodesics (straight lines) and Γ being a geodesic in the Riemannian manifold \mathbb{S}_{++}^n . More precisely, for each $\Sigma \in \mathbb{S}_{++}^n$ and each tangent vector $V \in \mathbb{S}^n$, the geodesic in the manifold \mathbb{S}_{++}^n emanating from Σ with direction V is given by

$$\Gamma(t) = (I + tL_\Sigma[V])\Sigma(I + tL_\Sigma[V]) \quad \text{for } t \in J^*, \quad (3.4)$$

where J^* is the open interval about the origin given by $J^* = \{t \in \mathbb{R} : I + tL_\Sigma[V] \in \mathbb{S}_{++}^n\}$ [Malagò *et al.*, 2018]. As a

consequence, for each point $(x, \mu, \Sigma) \in \mathcal{Z}$ and each tangent vector $(w, v, V) \in \mathbb{R}^m \times \mathbb{R}^n \times \mathbb{S}^n$, the Riemannian exponential map in \mathcal{Z} for $t \in J^*$ is given by

$$\exp_{(x, \mu, \Sigma)}(t(w, v, V)) := (\theta(t), \gamma(t), \Gamma(t)). \quad (3.5)$$

where $\theta(t) := x + tw$, $\gamma(t) := \mu + tv$, and $\Gamma(t)$ is defined by (3.4). By definition, $t \mapsto \exp_{(x, \mu, \Sigma)}(t(w, v, V))$ is the geodesic emanating from (x, μ, Σ) with direction (w, v, V) .

Given the Riemannian metric (3.3), one can define the corresponding notion of gradient and divergence [Lee, 2003]. For a differentiable function $\varphi : \mathcal{Z} \rightarrow \mathbb{R}$, its gradient $\tilde{\nabla}_d\varphi(z)$ w.r.t. the metric d defined by (3.1) is the unique element in the tangent space $\mathbb{R}^m \times \mathbb{R}^n \times \mathbb{S}^n$ satisfying

$$\langle \tilde{\nabla}_d\varphi(z), (w, v, V) \rangle_z = D\varphi_z(w, v, V)$$

for all $(w, v, V) \in \mathbb{R}^m \times \mathbb{R}^n \times \mathbb{S}^n$ with $D\varphi_z(w, v, V)$ denoting the standard directional derivative of φ at z in the direction (w, v, V) . By exploiting the special form of $\langle \cdot, \cdot \rangle_z$ in (3.3), we can compute $\tilde{\nabla}_d\varphi(z)$ explicitly:

Lemma 4 (Gradients). *For a differentiable function $\varphi : \mathcal{Z} \rightarrow \mathbb{R}$, we have for $z = (x, \mu, \Sigma)$ that*

$$\tilde{\nabla}_d\varphi(z) = (\nabla_x\varphi(z), \nabla_\mu\varphi(z), 2[\nabla_\Sigma\varphi(z)]\Sigma + 2\Sigma[\nabla_\Sigma\varphi(z)]), \quad (3.6)$$

where $(\nabla_x, \nabla_\mu, \nabla_\Sigma)$ are the standard (Euclidean) gradients of the respective components.

The last component in formula (3.6) for $\tilde{\nabla}_d\varphi$ reflects the curved geometry of \mathcal{Z} , and can be interpreted as the Riemannian gradient of the function $\Sigma \mapsto \varphi(x, \mu, \Sigma)$ w.r.t. the Bures distance \mathbb{B} .

For a continuous vector field $\Phi : \mathcal{Z} \rightarrow \mathbb{R}^m \times \mathbb{R}^n \times \mathbb{S}^n$ and a distribution $\rho \in \mathcal{P}(\mathcal{Z})$, the divergence $\text{div}_d(\rho\Phi)$ is the signed measure on \mathcal{Z} satisfying the integration by parts formula

$$\int_{\mathcal{Z}} \varphi(z) \text{div}_d(\rho\Phi)(dz) = - \int_{\mathcal{Z}} \langle \Phi(z), \tilde{\nabla}_d\varphi(z) \rangle_z \rho(dz)$$

for every differentiable function $\varphi : \mathcal{Z} \rightarrow \mathbb{R}$ with compact support. In case ρ has a density w.r.t. the Riemannian volume form on \mathcal{Z} , then this definition coincides with the standard divergence operator induced by Riemannian metric (3.3). The optimal transport distance and its induced Riemannian metric on the space $\mathcal{P}(\mathcal{Z})$ are relegated to Supplementary A.1

4 Gradient Flow for Maximum Mean Discrepancy

As $\mathcal{P}(\mathcal{Z})$ is an infinite dimensional curved space, many machine learning methods based on finite dimensional or linear structure cannot be directly applied to this manifold. To circumvent this problem, we use a positive definite kernel to map $\mathcal{P}(\mathcal{Z})$ to a RKHS and then perform our analysis on it. Let k be a positive definite kernel on \mathcal{Z} , and let \mathcal{H} be the RKHS generated by k . The inner product on \mathcal{H} is denoted by $\langle \cdot, \cdot \rangle_{\mathcal{H}}$, and the kernel mean embedding $\rho \in \mathcal{P}(\mathcal{Z}) \mapsto \mathbf{m}_\rho(\cdot) \in \mathcal{H}$ is given by $\mathbf{m}_\rho(z) := \int_{\mathcal{Z}} k(z, w) \rho(dw)$ for z in \mathcal{Z} . The MMD [Gretton *et al.*, 2012] between $\rho \in \mathcal{P}(\mathcal{Z})$ and the target ϱ is defined as the maximum of the mean difference between the

two distributions over all test functions in the unit ball of \mathcal{H} (see Supplementary A.3). Moreover, it can be expressed by $\text{MMD}(\rho, \varrho) = \|\mathbf{m}_\rho - \mathbf{m}_\varrho\|_{\mathcal{H}}$. When k is characteristic, the kernel mean embedding $\rho \mapsto \mathbf{m}_\rho$ is injective and therefore, $\text{MMD}(\rho, \varrho) = 0$ if and only if $\rho = \varrho$.

Consider the loss function $\mathcal{F}[\rho] := \frac{1}{2} \text{MMD}(\rho, \varrho)^2 = \frac{1}{2} \|\mathbf{m}_\rho - \mathbf{m}_\varrho\|_{\mathcal{H}}^2$. As explained in the introduction, there are three advantages of MMD over Kullback-Leibler divergence: its associated gradient flow can employ a sample approximation for the target distribution, the input distribution ρ does not have to be absolutely continuous w.r.t. the target distribution ϱ , and the squared MMD possesses unbiased sample gradients. For each ρ , the Riemannian gradient $\text{grad } \mathcal{F}[\rho]$ is defined as the unique element in $T_\rho \mathcal{P}(\mathcal{Z})$ satisfying $g_\rho(\text{grad } \mathcal{F}[\rho], \zeta) = \left. \frac{d}{dt} \right|_{t=0} \mathcal{F}[\rho_t]$ for every differentiable curve $t \mapsto \rho_t \in \mathcal{P}(\mathcal{Z})$ passing through ρ at $t = 0$ with tangent vector $\left. \partial_t \rho_t \right|_{t=0} = \zeta$. By using the Riemannian metric tensor (A.3), we can compute explicitly this gradient.

Lemma 5 (Gradient formula). *The Riemannian gradient of \mathcal{F} satisfies $\text{grad } \mathcal{F}[\rho] = -\text{div}_d(\rho \tilde{\nabla}_d[\mathbf{m}_\rho - \mathbf{m}_\varrho])$.*

The Riemannian gradient $\text{grad } \mathcal{F}$ on $\mathcal{P}(\mathcal{Z})$ depends not only on the gradient operator $\tilde{\nabla}_d$ but also on the divergence operator. Using Lemma 5, we can rewrite the gradient flow equation $\partial_t \rho_t = -\text{grad } \mathcal{F}[\rho_t]$ explicitly as

$$\partial_t \rho_t = \text{div}_d(\rho_t \tilde{\nabla}_d[\mathbf{m}_{\rho_t} - \mathbf{m}_\varrho]) \quad \text{for } t \geq 0. \quad (4.1)$$

The next result exhibits the rate at which \mathcal{F} decreases its value along the flow.

Proposition 6 (Rate of decrease). *Along the gradient flow $t \mapsto \rho_t \in \mathcal{P}(\mathcal{Z})$ given by (4.1), we have*

$$\frac{d}{dt} \mathcal{F}[\rho_t] = - \int_{\mathcal{Z}} \|\tilde{\nabla}_d[\mathbf{m}_{\rho_t} - \mathbf{m}_\varrho]\|_z^2 \rho_t(dz) \quad \text{for } t \geq 0.$$

Proposition 6 implies that $\left. \frac{d}{dt} \mathcal{F}[\rho_t] \right|_{t=0} = 0$ if and only if $\tilde{\nabla}_d[\mathbf{m}_{\rho_t} - \mathbf{m}_\varrho](z) = 0$ for every z in the support of the distribution ρ_t . Thus, the objective function will decrease whenever the gradient $\tilde{\nabla}_d[\mathbf{m}_{\rho_t} - \mathbf{m}_\varrho]$ is not identically zero.

4.1 Riemannian Forward Euler Scheme

We propose the Riemannian version of the forward Euler scheme to discretize continuous flow (4.1):

$$\begin{aligned} \rho^{\tau+1} &= \exp(s_\tau \Phi^\tau) \# \rho^\tau \\ \text{with } \Phi^\tau &:= -\tilde{\nabla}_d[\mathbf{m}_{\rho^\tau} - \mathbf{m}_\varrho], \end{aligned} \quad (4.2)$$

where $s_\tau > 0$ is the step size. Here, for a vector field $\Phi = (\Phi_1, \Phi_2, \Phi_3) : \mathcal{Z} \rightarrow \mathbb{R}^m \times \mathbb{R}^n \times \mathbb{S}^n$ and for $\varepsilon \geq 0$, $\exp(\varepsilon \Phi) : \mathcal{Z} \rightarrow \mathcal{Z}$ is the Riemannian exponential map induced by (3.5), i.e., for $z = (x, \mu, \Sigma) \in \mathcal{Z}$:

$$\exp_z(\varepsilon \Phi(z)) = \begin{pmatrix} x + \varepsilon \Phi_1(z) \\ \mu + \varepsilon \Phi_2(z) \\ (I + \varepsilon L_\Sigma[\Phi_3(z)]) \Sigma (I + \varepsilon L_\Sigma[\Phi_3(z)]) \end{pmatrix}.$$

Algorithm 1 Discretized Gradient Flow Algorithm for Scheme (4.2)

- 1: **Input:** a source distribution $\rho^0 = N^{-1} \sum_{i=1}^N \delta_{z_i^0}$, a target distribution $\varrho = M^{-1} \sum_{j=1}^M \delta_{\bar{z}_j}$, a number of iterations T , a sequence of step sizes $s_\tau > 0$ with $\tau = 0, 1, \dots, T$ and a kernel k
- 2: **Initialization:** Compute $\bar{\Psi}(z) = M^{-1} \sum_{j=1}^M \tilde{\nabla}_d^1 k(z, \bar{z}_j)$ with $\tilde{\nabla}_d^1 k(z, \bar{z}_j)$ is $\tilde{\nabla}_d$ of $z \mapsto k(z, \bar{z}_j)$
- 3: **repeat for each** $\tau = 0, \dots, T - 1$:
- 4: Compute $\Psi^\tau(z) = N^{-1} \sum_{i=1}^N \tilde{\nabla}_d^1 k(z, z_i^\tau)$
- 5: **for** $i = 1, \dots, N$
- 6: **do** $z_i^{\tau+1} \leftarrow \exp_{z_i^\tau}(s_\tau(\bar{\Psi} - \Psi^\tau)(z_i^\tau))$
- 7: **end for**
- 8: **Output:** $\rho^T = N^{-1} \sum_{i=1}^N \delta_{z_i^T}$

Notice in the above equation that the input z affects simultaneously the bases of the exponential map \exp_z as well as the direction $\Phi(z)$. This map is the ε -perturbation of the identity map along geodesics with directions Φ . When $\rho^\tau = N^{-1} \sum_{i=1}^N \delta_{z_i^\tau}$ is an empirical distribution, scheme (4.2) flows each particle z_i^τ to the new position $z_i^{\tau+1} = \exp_{z_i^\tau}(s_\tau \Phi(z_i^\tau))$. The next lemma shows that Φ^τ is the steepest descent direction for \mathcal{F} w.r.t. the exponential map among all directions in the space $\mathbb{L}^2(\rho^\tau)$, which is the collection of all vector fields Φ on \mathcal{Z} satisfying $\|\Phi\|_{\mathbb{L}^2(\rho^\tau)}^2 := \int_{\mathcal{Z}} \|\Phi(z)\|_z^2 \rho^\tau(dz) < \infty$.

Lemma 7 (Steepest descent direction). *Fix a distribution $\rho^\tau \in \mathcal{P}(\mathcal{Z})$. For any vector field $\Phi : \mathcal{Z} \rightarrow \mathbb{R}^m \times \mathbb{R}^n \times \mathbb{S}^n$, we have*

$$\left. \frac{d}{d\varepsilon} \right|_{\varepsilon=0} \mathcal{F}[\exp(\varepsilon \Phi) \# \rho^\tau] = \int_{\mathcal{Z}} \tilde{\nabla}_d[\mathbf{m}_{\rho^\tau} - \mathbf{m}_\varrho](z), \Phi(z)_z \rho^\tau(dz).$$

If $\hat{\Phi}^\tau$ is the unit vector field (w.r.t. the $\|\cdot\|_{\mathbb{L}^2(\rho^\tau)}$ norm) in the direction of Φ^τ given in (4.2), then

$$\left. \frac{d}{d\varepsilon} \right|_{\varepsilon=0} \mathcal{F}[\exp(\varepsilon \hat{\Phi}^\tau) \# \rho^\tau] = -\|\tilde{\nabla}_d[\mathbf{m}_{\rho^\tau} - \mathbf{m}_\varrho]\|_{\mathbb{L}^2(\rho^\tau)}$$

and this is the fastest decay rate among all unit directions Φ in $\mathbb{L}^2(\rho^\tau)$.

It follows from Lemma 7 that the discrete scheme (4.2) satisfies the Riemannian gradient descent property: if $\tilde{\nabla}_d[\mathbf{m}_{\rho^\tau} - \mathbf{m}_\varrho]$ is nonzero and if $s_\tau > 0$ is chosen sufficiently small, then $\mathcal{F}[\rho^{\tau+1}] < \mathcal{F}[\rho^\tau]$. In Proposition 14 in the Supplementary, we quantify the amount of decrease of \mathcal{F} at each iteration. Algorithm 1 implements the flow (4.2) iteratively. Each iteration in Algorithm 1 has complexity $O(N(Nm + n^3))$, where m is the feature's dimension, n is the reduced dimension ($n \ll m$), N is the number of particles.

Convergence. We now study the (weak) convergence of the solution ρ_t of the continuous gradient flow (4.1), as well as the discretized counterpart ρ^τ of flow (4.2), to the target distribution ϱ . When the kernel k is characteristic, this convergence is equivalent to $\lim_{t \rightarrow \infty} \text{MMD}(\rho_t, \varrho) = 0$. Because the objective function \mathcal{F} is not displacement convex [Arbel *et al.*, 2019, Section 3.1], the convergent theory for gradient flows

in [Ambrosio *et al.*, 2008] does not apply even in the case of Euclidean spaces. In general, there is a possibility that $\text{MMD}(\rho_t, \varrho)$ does not decrease to zero as $t \rightarrow \infty$. In view of Proposition 6, this happens if the solutions ρ_t are trapped inside the set $\{\rho : \int_{\mathcal{Z}} \|\tilde{\nabla}_d[\mathbf{m}_\rho - \mathbf{m}_\varrho]\|_z^2 \rho(dz) = 0\}$. For each distribution ρ on \mathcal{Z} , we define in Supplementary A.3 a symmetric linear and positive operator $\mathbb{K}_\rho : \mathcal{H} \rightarrow \mathcal{H}$ with the property that $\langle \mathbb{K}_\rho[\mathbf{m}_\rho - \mathbf{m}_\varrho], \mathbf{m}_\rho - \mathbf{m}_\varrho \rangle_{\mathcal{H}} = \int_{\mathcal{Z}} \|\tilde{\nabla}_d[\mathbf{m}_\rho - \mathbf{m}_\varrho]\|_z^2 \rho(dz)$. We further show in Proposition 16 that ρ_t globally converges in MMD if the minimum eigenvalue λ_t of the operator \mathbb{K}_{ρ_t} satisfies an integrability condition.

4.2 Noisy Riemannian Forward Euler Scheme

The analysis in Section 4.1 reveals that the gradient flows suffer from convergence issues if the residual $\mathbf{m}_{\rho_t} - \mathbf{m}_\varrho$ belongs to the null space of the operator \mathbb{K}_{ρ_t} . To resolve this, we employ graduated optimization [Arbel *et al.*, 2019; Gulcehre *et al.*, 2016; Gulcehre *et al.*, 2017; Hazan *et al.*, 2016] used for non-convex optimization in Euclidean spaces. Specifically, we modify algorithm (4.2) by injecting Gaussian noise into the exponential map at each iteration τ to obtain

$$\begin{aligned} \rho^{\tau+1} &= \exp(s_\tau \Phi^\tau)_{\#} \rho^{\tau, \beta_\tau} \\ \text{with } f^{\beta_\tau} : (z, u) &\mapsto \exp_z(\beta_\tau u), \quad \rho^{\tau, \beta_\tau} := f^{\beta_\tau}_{\#}(\rho^\tau \otimes g). \end{aligned} \quad (4.3)$$

Here g is a Gaussian measure with distribution $\mathcal{N}_{\mathbb{R}^m}(0, 1) \otimes \mathcal{N}_{\mathbb{R}^n}(0, 1) \otimes \mathcal{N}_{\mathbb{S}^n}(0, 1)$ on the tangent space and $\mathcal{N}_{\mathbb{S}^n}(0, 1)$ denotes an n -by- n symmetric matrix whose upper triangular elements are i.i.d. standard Gaussian random variables. When $\rho^\tau = N^{-1} \sum_{i=1}^N \delta_{z_i^\tau}$, scheme (4.3) flows each particle z_i^τ first to $z_i^{\tau, \beta_\tau} := \exp_{z_i^\tau}(\beta_\tau U)$ with noise $U \sim g$ and then to $z_i^{\tau+1} = \exp_{z_i^{\tau, \beta_\tau}}(s_\tau \Phi(z_i^{\tau, \beta_\tau}))$. Our next result extends Proposition 8 in [Arbel *et al.*, 2019] for the standard quadratic cost on the Euclidean space to the nonstandard cost function d^2 on the curved Riemannian manifold \mathcal{Z}_{++} . It demonstrates that scheme (4.3) achieves the global minimum of \mathcal{F} provided that k is a Lipschitz-gradient kernel and both the noise level β_τ and the step size s_τ are well controlled. The proof of Proposition 8 is given in Supplementary A.3 and relies on arguments that are different from that of [Arbel *et al.*, 2019].

Proposition 8 (Objective value decay for noisy scheme). *Suppose that k is a Lipschitz-gradient kernel¹ with constant L , and the noise level β_τ satisfies*

$$\lambda \beta_\tau^2 \mathcal{F}[\rho^\tau] \leq \int_{\mathcal{Z}} \|\Phi^\tau(z)\|_z^2 \rho^{\tau, \beta_\tau}(dz) \quad (4.4)$$

for some constant $\lambda > 0$. Then for $\rho^{\tau+1}$ obtained from scheme (4.3), we have

$$\mathcal{F}[\rho^{\tau+1}] \leq \mathcal{F}[\rho^0] \exp\left(-\lambda \sum_{i=0}^{\tau} [s_i(1 - 2Ls_i)\beta_i^2]\right).$$

In particular, $\mathcal{F}[\rho^\tau]$ tends to zero if the sequence $\sum_{i=0}^{\tau} s_i(1 - 2Ls_i)\beta_i^2$ goes to positive infinity. For an adaptive step size $s_\tau \leq 1/4L$, this condition is met if, for example,

¹See Definition A.3 for the technical definition

β_τ is chosen of the form $(\tau s_\tau)^{-\frac{1}{2}}$ while still satisfying (4.4). The noise perturbs the direction of descent, whereas the step size determines how far to move along this perturbed direction. The noise level needs to be adjusted so that the gradient is not too blurred, but it does not necessarily decrease at each iteration. When the incumbent distribution ρ^τ is close to a local optimum, it is helpful to increase the noise level to escape the local optimum. We demonstrate in Lemma 13 in the Supplementary that any positive definite kernel k with bounded Hessian w.r.t. distance d is a Lipschitz-gradient kernel. Algorithm 3 in the Supplementary describes (4.3) in details.

5 Numerical Experiments

We evaluate the proposed gradient flow on real-world datasets and then illustrate its applications in transfer learning. We augment samples for the target dataset, where only a few samples in the dataset are available. We consider three datasets: the MNIST (M) [LeCun and Cortes, 2010], Fashion-MNIST (F) [Xiao *et al.*, 2017], Kuzushiji-MNIST (K) [Clanuwat *et al.*, 2018]. To satisfy the Gaussianity assumption of the conditional distributions, we cluster all the images from each class of the datasets and keep the largest cluster for each class. To demonstrate the scalability of our algorithm to higher-dimensional images, we run experiments on Tiny ImageNet (TIN) [Russakovsky *et al.*, 2015] and upscaled SVHN [Netzer *et al.*, 2011] datasets, where images are of $3 \times 64 \times 64$ size.

Our mapping ϕ is from \mathbb{R}^m to \mathbb{R}^2 in the lifting procedure. To compute the MMD distance using kernel embeddings, we use a tensor kernel k on \mathcal{Z} composed from three standard Gaussian kernels corresponding for each component of the feature space \mathbb{R}^m , the mean space \mathbb{R}^2 and the covariance matrix space \mathbb{S}_{++}^2 . As a consequence, k is a characteristic kernel by [Szabó and Sriperumbudur, 2018, Theorem 4].

Experiment: Gradient Flow between Datasets. We visualize the path travelled by each sample from the source domain to the target domain, as depicted in Fig. 2. We draw randomly $N = 200$ images equally for 10 classes of the source domain, and $M = 50$ images equally for 10 classes of the target domain ($M = 10$ for the TIN and SVHN datasets). In each subfigure, each column represents a snapshot of a certain time-step and the samples flow from the source (left) to the target (right) as the number of steps increases. The first column in Fig. 2 are the images from the source domain, where the gradient flows start. Empirically, the algorithm converges after step 140 for *NIST datasets and step 6000 for TIN and SVHN. The experiments are run on a C5.4xlarge AWS instance (a CPU instance) and all finish within one hour.

5.1 Application in Transfer Learning

Our gradient flow can alleviate the problem of insufficient labeled data by synthesizing new samples to augment the target dataset. In this section, we demonstrate that the generated target domain samples can improve the accuracy in one-shot and five-shot transfer learning tasks.

First, we fix a source domain and pretrain a classifier P on this domain. We draw randomly N samples from the source domain to form the source dataset $(x_i, y_i)_{i=1}^N$. Next, we pick a target domain and draw randomly a few samples from this

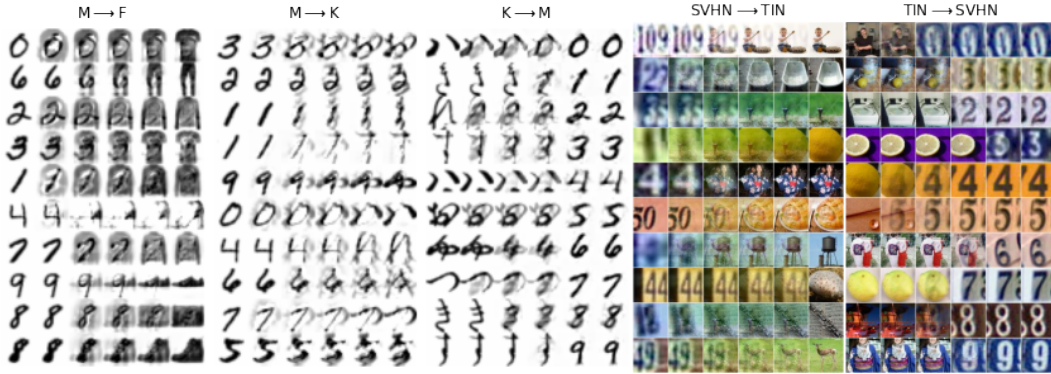


Figure 2: Sample path visualizations for five pairs of source-target domain. The original image and additional results are in the supplementary.

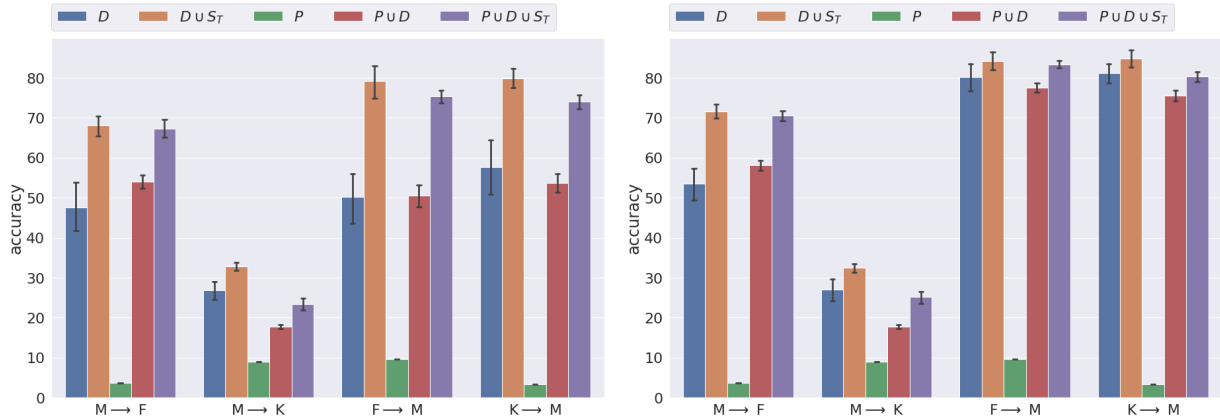


Figure 3: Average target domain accuracy on the test split for transfer learning with one-shot (left) and five-shot (right). Results are taken over 10 independent replications, and the range of accuracy is displayed by the error bars.

target domain: for example, in 1-shot learning, only 1 image per class from the target domain is selected to form the target dataset $D = (\bar{x}_j, \bar{y}_j)_{j=1}^M$. We then perform a noisy gradient flow scheme (4.3) from the source dataset to the target dataset to get N new samples $S_T = (x_i^T, y_i^T)_{i=1}^N$. With the target dataset D and new samples S_T , we can retrain the classifier P . Similarly, we can also train new classifiers from scratch using datasets D and $D \cup S_T$. Finally, we test the classifiers on the test set of the target domain.

Fig. 3 presents the accuracy of five transfer learning strategies on four pairs of source and target domain. For the labels above the plot, labels without P mean training a new classifier from scratch, whereas labels with P mean transferring the pre-trained classifier. D and S_T represent the samples in the target domain and our flowed samples. We observe a common trend that the addition of the flowed samples S_T always improves the accuracy of the classifiers, as we compare $D \cup S_T$ with D and compare $P \cup D \cup S_T$ with $P \cup D$. Moreover, the data augmentation with S_T leads to a higher increase of accuracy for the 1-shot learning, where the data scarcity problem is more severe. The transfer learning results for SVHN and TIN datasets are provided in the Supplementary B.7. Although Few-shot learning is more challenging due to the high com-

plexity of the datasets, the addition of S_T still improves the accuracy. We also compare with [Alvarez-Melis and Fusi, 2021]², mixup method [Zhang *et al.*, 2017], and image augmentation methods, see results in Supplementary B.8–B.10.

Conclusions. This paper focuses on a gradient flow approach to generate new labeled data samples in the target domain. To overcome the discrete nature of the labels, we represent datasets as distributions on the feature-Gaussian space, and the flow is formulated to minimize the MMD loss function under an optimal transport metric. Contrary to existing gradient flows on linear structure, our flows are developed on the *curved* Riemannian manifold of Gaussian distributions. We provide explicit formula for the Riemannian gradient of the MMD loss, and analyze in details the flow equations and the convergence properties of both continuous and discretized forms. The numerical experiments demonstrate that our method can efficiently generate high-fidelity labeled training data for real-world datasets, and improve the classification accuracy in few-shot learning. The main limitation exists in the assumption that the data of one label forms an elliptical distribution.

²The only gradient flow work that has experiments on *NIST datasets, but it does not run experiments on TIN and SVHN.

Ethical Statement

Our work has positive societal impacts, because it can help reduce repetitive data collection and labeling work. It does not have possible negative societal impacts in the current stage.

References

- [Alvarez-Melis and Fusi, 2020] David Alvarez-Melis and Nicolo Fusi. Geometric dataset distances via optimal transport. In *Advances in Neural Information Processing Systems*, volume 33, pages 21428–21439, 2020.
- [Alvarez-Melis and Fusi, 2021] David Alvarez-Melis and Nicolò Fusi. Dataset dynamics via gradient flows in probability space. In *Proceedings of the 38th International Conference on Machine Learning*, volume 139, pages 219–230, 2021.
- [Ambrosio *et al.*, 2008] L. Ambrosio, N. Gigli, and G. Savaré. *Gradient Flows in Metric Spaces and in the Space of Probability Measures*. Birkhäuser Verlag, 2008.
- [Arbel *et al.*, 2019] Michael Arbel, Anna Korba, Adil Salim, and Arthur Gretton. Maximum mean discrepancy gradient flow. In *Advances in Neural Information Processing Systems*, volume 32, pages 6481–6491, 2019.
- [Arbel *et al.*, 2020] M Arbel, A Gretton, W Li, and G Montufar. Kernelized Wasserstein natural gradient. In *International Conference on Learning Representations*, 2020.
- [Bellemare *et al.*, 2017] Marc G. Bellemare, Ivo Danihelka, Will Dabney, Shakir Mohamed, Balaji Lakshminarayanan, Stephan Hoyer, and Remi Munos. The Cramer distance as a solution to biased Wasserstein gradients. *arXiv preprint arXiv:1705.10743*, 2017.
- [Benamou and Brenier, 2000] Jean-David Benamou and Yann Brenier. A computational fluid mechanics solution to the Monge-Kantorovich mass transfer problem. *Numerische Mathematik*, 2000.
- [Bhatia *et al.*, 2019] R. Bhatia, T. Jain, and Y. Lim. On the Bures-Wasserstein distance between positive definite matrices. *Expositiones Mathematicae*, 37(2):165–191, 2019.
- [Bhatia, 1997] Rajendra Bhatia. *Matrix Analysis*. Springer, 1997.
- [Bińkowski *et al.*, 2018] Mikołaj Bińkowski, Danica J. Sutherland, Michael Arbel, and Arthur Gretton. Demystifying MMD GANs. In *International Conference on Learning Representations*, 2018.
- [Chen and Li, 2018] Yifan Chen and Wuchen Li. Optimal transport natural gradient for statistical manifolds with continuous sample space. In *Information Geometry*, 2018.
- [Chizat and Bach, 2018] Lénaïc Chizat and Francis Bach. On the global convergence of gradient descent for over-parameterized models using optimal transport. In *Advances in Neural Information Processing Systems*, volume 31, 2018.
- [Clanuwat *et al.*, 2018] Tarin Clanuwat, Mikel Bober-Irizar, Asanobu Kitamoto, Alex Lamb, Kazuaki Yamamoto, and David Ha. Deep learning for classical Japanese literature. *arXiv preprint arXiv:1812.01718*, 2018.
- [Courty *et al.*, 2017] Nicolas Courty, Rémi Flamary, Amaury Habrard, and Alain Rakotomamonjy. Joint distribution optimal transportation for domain adaptation. In *Advances in Neural Information Processing Systems*, volume 30, 2017.
- [Damodaran *et al.*, 2018] Bharath Bhushan Damodaran, Benjamin Kellenberger, Rémi Flamary, Devis Tuia, and Nicolas Courty. DeepJDOT: Deep joint distribution optimal transport for unsupervised domain adaptation. In *Proceedings of the European Conference on Computer Vision (ECCV)*, pages 447–463, 2018.
- [Fan and Alvarez-Melis, 2022] Jiaojiao Fan and David Alvarez-Melis. Generating synthetic datasets by interpolating along generalized geodesics. In *NeurIPS 2022 Workshop on Synthetic Data for Empowering ML Research*, 2022.
- [Frogner and Poggio, 2020] Charlie Frogner and Tomaso Poggio. Approximate inference with Wasserstein gradient flows. In *International Conference on Artificial Intelligence and Statistics*, pages 2581–2590. PMLR, 2020.
- [Gao *et al.*, 2018] Hang Gao, Zheng Shou, Alireza Zareian, Hanwang Zhang, and Shih-Fu Chang. Low-shot learning via covariance-preserving adversarial augmentation networks. *Advances in Neural Information Processing Systems*, 31, 2018.
- [Gelbrich, 1990] M. Gelbrich. On a formula for the L^2 Wasserstein metric between measures on Euclidean and Hilbert spaces. *Mathematische Nachrichten*, 147(1):185–203, 1990.
- [Gretton *et al.*, 2012] Arthur Gretton, Karsten M. Borgwardt, Malte J. Rasch, Bernhard Schölkopf, and Alexander Smola. A kernel two-sample test. *Journal of Machine Learning Research*, 13(25):723–773, 2012.
- [Gulcehre *et al.*, 2016] Caglar Gulcehre, Marcin Moczulski, Misha Denil, and Yoshua Bengio. Noisy activation functions. In *Proceedings of The 33rd International Conference on Machine Learning*, pages 3059–3068, 2016.
- [Gulcehre *et al.*, 2017] Caglar Gulcehre, Marcin Moczulski, Francesco Visin, and Yoshua Bengio. Mollifying networks. In *5th International Conference on Learning Representations*, 2017.
- [Hazan *et al.*, 2016] Elad Hazan, Kfir Yehuda Levy, and Shai Shalev-Shwartz. On graduated optimization for stochastic non-convex problems. In *Proceedings of The 33rd International Conference on Machine Learning*, pages 1833–1841, 2016.
- [Hinton *et al.*, 2012] Geoffrey Hinton, Nitish Srivastava, and Kevin Swersky. Neural networks for machine learning, Lecture 6a: Overview of mini-batch gradient descent. 2012.
- [Jordan *et al.*, 1998] R. Jordan, D. Kinderlehrer, and F. Otto. The variational formulation of the Fokker–Planck equation. *SIAM Journal on Mathematical Analysis*, 29:1–17, 1998.
- [LeCun and Cortes, 2010] Yann LeCun and Corinna Cortes. MNIST handwritten digit database. 2010.
- [Lee, 2003] John Lee. *Introduction to Smooth Manifolds*. Springer-Verlag, 2003.

- [Liu and Wang, 2016] Qiang Liu and Dilin Wang. Stein variational gradient descent: A general purpose Bayesian inference algorithm. In *Advances in Neural Information Processing Systems*, volume 29, 2016.
- [Liu, 2017] Qiang Liu. Stein variational gradient descent as gradient flow. In *Advances in Neural Information Processing Systems*, volume 30, 2017.
- [Liutkus *et al.*, 2019] Antoine Liutkus, Umut Simsekli, Szymon Majewski, Alain Durmus, and Fabian-Robert Stöter. Sliced-Wasserstein flows: Nonparametric generative modeling via optimal transport and diffusions. In *Proceedings of the 36th International Conference on Machine Learning*, 2019.
- [Malagò *et al.*, 2018] L. Malagò, L. Montrucchio, and G. Pistone. Wasserstein Riemannian geometry of Gaussian densities. *Information Geometry*, 1(2):137–179, 2018.
- [Moreno-Barea *et al.*, 2018] Francisco J. Moreno-Barea, Fiammetta Strazzer, José M. Jerez, Daniel Urda, and Leonardo Franco. Forward noise adjustment scheme for data augmentation. In *2018 IEEE Symposium Series on Computational Intelligence (SSCI)*, pages 728–734, 2018.
- [Mroueh and Nguyen, 2021] Youssef Mroueh and Truyen Nguyen. On the convergence of gradient descent in GANs: MMD GAN as a gradient flow. In *International Conference on Artificial Intelligence and Statistics*, 2021.
- [Mroueh *et al.*, 2019] Youssef Mroueh, Tom Sercu, and Anant Raj. Sobolev descent. In *Proceedings of the Twenty-Second International Conference on Artificial Intelligence and Statistics*, pages 2976–2985, 2019.
- [Netzer *et al.*, 2011] Yuval Netzer, Tao Wang, Adam Coates, Alessandro Bissacco, Bo Wu, and Andrew Y Ng. Reading digits in natural images with unsupervised feature learning. 2011.
- [Otto, 2001] F. Otto. The geometry of dissipative evolution equations: the porous medium equation. *Comm. Partial Differential Equations*, 26:101–174, 2001.
- [Rezende *et al.*, 2016] Danilo Rezende, Ivo Danihelka, Karol Gregor, Daan Wierstra, et al. One-shot generalization in deep generative models. In *International conference on machine learning*, pages 1521–1529. PMLR, 2016.
- [Russakovsky *et al.*, 2015] Olga Russakovsky, Jia Deng, Hao Su, Jonathan Krause, Sanjeev Satheesh, Sean Ma, Zhiheng Huang, Andrej Karpathy, Aditya Khosla, Michael Bernstein, et al. Imagenet large scale visual recognition challenge. *International journal of computer vision*, 115(3):211–252, 2015.
- [Santambrogio, 2015] Filippo Santambrogio. *Optimal Transport for Applied Mathematicians: Calculus of Variations, PDEs and Modeling*. Birkhäuser, 2015.
- [Santambrogio, 2017] Filippo Santambrogio. Euclidean, metric, and Wasserstein gradient flows: An overview. *Bulletin of Mathematical Sciences*, 7:87–154, 2017.
- [Shorten and Khoshgoftaar, 2019] Connor Shorten and Taghi M Khoshgoftaar. A survey on image data augmentation for deep learning. *Journal of big data*, 6(1):1–48, 2019.
- [Szabó and Sriperumbudur, 2018] Zoltán Szabó and Bharath K. Sriperumbudur. Characteristic and universal tensor product kernels. *Journal of Machine Learning Research*, 18(233):1–29, 2018.
- [Takatsu, 2011] Asuka Takatsu. Wasserstein geometry of Gaussian measures. *Osaka Journal of Mathematics*, 48(4):1005–1026, 2011.
- [van der Maaten and Hinton, 2008] Laurens van der Maaten and Geoffrey Hinton. Visualizing data using t-SNE. *Journal of Machine Learning Research*, 9:2579–2605, 2008.
- [Villani, 2008] C. Villani. *Optimal Transport: Old and New*. Springer Science & Business Media, 2008.
- [Wang *et al.*, 2020] Yaqing Wang, Quanming Yao, James T Kwok, and Lionel M Ni. Generalizing from a few examples: A survey on few-shot learning. *ACM computing surveys (csur)*, 53(3):1–34, 2020.
- [Wang *et al.*, 2021] Gefei Wang, Yuling Jiao, Qian Xu, Yang Wang, and Can Yang. Deep generative learning via Schrödinger bridge. In Marina Meila and Tong Zhang, editors, *Proceedings of the 38th International Conference on Machine Learning*, volume 139 of *Proceedings of Machine Learning Research*, pages 10794–10804. PMLR, 18–24 Jul 2021.
- [Wiatrak *et al.*, 2019] Maciej Wiatrak, Stefano V Albrecht, and Andrew Nystrom. Stabilizing generative adversarial networks: A survey. *arXiv preprint arXiv:1910.00927*, 2019.
- [Xiao *et al.*, 2017] Han Xiao, Kashif Rasul, and Roland Vollgraf. Fashion-mnist: a novel image dataset for benchmarking machine learning algorithms. *arXiv preprint arXiv:1708.07747*, 2017.
- [Yi *et al.*, 2019] Xin Yi, Ekta Walia, and Paul Babyn. Generative adversarial network in medical imaging: A review. *Medical Image Analysis*, 58:101552, 2019.
- [Zhang *et al.*, 2017] Hongyi Zhang, Moustapha Cisse, Yann N Dauphin, and David Lopez-Paz. mixup: Beyond empirical risk minimization. *arXiv preprint arXiv:1710.09412*, 2017.

The Supplementary Material is organized into two parts. In Section A, we provide the proofs and further discussions of the results in the main paper. Section B includes implementation details as well as additional numerical results. All the models and data used to create the results in the paper are in the supplementary file.

A Proofs

A.1 Optimal Transport and Riemannian Structure on $\mathcal{P}(\mathcal{Z})$

To define a gradient flow for probability distributions on \mathcal{Z} , it is essential to have a concept of gradients for functionals defined on $\mathcal{P}(\mathcal{Z})$. This requires a meaningful Riemannian structure on $\mathcal{P}(\mathcal{Z})$, and here, we adopt a Riemannian structure generated by the optimal transport on $\mathcal{P}(\mathcal{Z})$ with ground cost d^2 . The optimal transport metric $\mathbb{W}(\rho_0, \rho_1)$ between any two distributions $\rho_0, \rho_1 \in \mathcal{P}(\mathcal{Z})$ is defined by formula (A.7) of Appendix A.2. As (\mathcal{Z}, d) is a Riemannian manifold by Proposition 3, it follows from the celebrated Benamou-Brenier formula [Benamou and Brenier, 2000] that \mathbb{W} can be expressed in terms of a dynamic formulation. Precisely,

$$\mathbb{W}(\rho_0, \rho_1)^2 = \inf_{(\rho, \phi) \in \mathcal{A}(\rho_0, \rho_1)} \int_0^1 \int_{\mathcal{Z}} \|\tilde{\nabla}_d \phi_t(z)\|_z^2 \rho_t(dz) dt, \quad (\text{A.1})$$

where $\mathcal{A}(\rho_0, \rho_1)$ is the collection of all pairs (ρ, ϕ) of curve $\rho : [0, 1] \rightarrow \mathcal{P}(\mathcal{Z})$ with endpoints ρ_0 and ρ_1 , and function $\phi : [0, 1] \times \mathcal{Z} \rightarrow \mathbb{R}$ that satisfies the continuity equation

$$\partial_t \rho + \text{div}_d(\rho_t \tilde{\nabla}_d \phi_t) = 0 \quad (\text{A.2})$$

in the sense of distributions in $(0, 1) \times \mathcal{Z}$. For brevity, hereafter ρ_t and ϕ_t denote functions in the z variable defined by $\rho_t(z) = \rho(t, z)$ and $\phi_t(z) = \phi(t, z)$.

Riemannian metric on $\mathcal{P}(\mathcal{Z})$. The formulation (A.1) gives rise to the following Riemannian structure on $\mathcal{P}(\mathcal{Z})$ induced by distance \mathbb{W} . First, the continuity equation enables us to identify a tangent vector $\partial_t \rho$ with the divergence $-\text{div}_d(\rho_t \tilde{\nabla}_d \phi_t)$. Thus the tangent space of $\mathcal{P}(\mathcal{Z})$ at a distribution ρ can be defined as $T_\rho \mathcal{P}(\mathcal{Z}) := \{ -\text{div}_d(\rho \tilde{\nabla}_d \varphi) : \varphi \text{ is a differentiable function with compact support on } \mathcal{Z} \}$. Second, we let $g_\rho : T_\rho \mathcal{P}(\mathcal{Z}) \times T_\rho \mathcal{P}(\mathcal{Z}) \rightarrow \mathbb{R}$ be the Riemannian metric tensor given by

$$g_\rho(\zeta_1, \zeta_2) := \int_{\mathcal{Z}} \langle \tilde{\nabla}_d \varphi_1(z), \tilde{\nabla}_d \varphi_2(z) \rangle_z \rho(dz) \quad (\text{A.3})$$

for $\zeta_1 = -\text{div}_d(\rho \tilde{\nabla}_d \varphi_1)$ and $\zeta_2 = -\text{div}_d(\rho \tilde{\nabla}_d \varphi_2)$. With this definition and due to (A.2), formula (A.1) can be rewritten using the metric tensor as

$$\mathbb{W}(\rho_0, \rho_1)^2 = \inf_{(\rho, \phi) \in \mathcal{A}(\rho_0, \rho_1)} \int_0^1 g_{\rho_t}(\partial_t \rho, \partial_t \rho) dt.$$

The metric tensor (A.3) allows us to define a notion of Riemannian gradients for functionals on $\mathcal{P}(\mathcal{Z})$. In the next section we shall compute this gradient explicitly for the squared MMD gradient flow.

A.2 Proofs and Results related to Section 3

For Proposition 3. Recall that the Bures distance defined on \mathbb{S}_{++}^n is

$$\mathbb{B}(\Sigma_1, \Sigma_2) := \left[\text{tr}(\Sigma_1 + \Sigma_2 - 2[\Sigma_1^{\frac{1}{2}} \Sigma_2 \Sigma_1^{\frac{1}{2}}]^{\frac{1}{2}}) \right]^{\frac{1}{2}}, \quad (\text{A.4})$$

and $\tilde{\nabla}_d \varphi(z)$ is the unique element in the tangent space $\mathbb{R}^m \times \mathbb{R}^n \times \mathbb{S}^n$ satisfying

$$\langle \tilde{\nabla}_d \varphi(z), (w, v, V) \rangle_z = D\varphi_z(w, v, V) \quad \text{for all } (w, v, V) \in \mathbb{R}^m \times \mathbb{R}^n \times \mathbb{S}^n. \quad (\text{A.5})$$

The proof of Proposition 3 relies on the following result from [Takatsu, 2011, Proposition A] (see also [Bhatia *et al.*, 2019, Theorem 5] and [Malagò *et al.*, 2018, Proposition 6]).

Proposition 9. *The space \mathbb{S}_{++}^n is a Riemannian manifold with the following structures: at each point $\Sigma \in \mathbb{S}_{++}^n$, the tangent space is $T_\Sigma \mathbb{S}_{++}^n = \mathbb{S}^n$ and the Riemannian metric is given by*

$$\langle X, Y \rangle_\Sigma := \text{tr} \left(L_\Sigma[X] \Sigma L_\Sigma[Y] \right) = \frac{1}{2} \langle L_\Sigma[X], Y \rangle \quad \text{for } X, Y \in \mathbb{S}^n.$$

Moreover, the distance function corresponding to this Riemannian metric coincides with the Bures distance \mathbb{B} given by (A.4).

We are now ready to prove Proposition 3.

Proof of Proposition 3. As a consequence of Proposition 9, \mathcal{Z} is the product Riemannian manifold with tangent space $T_{(x, \mu, \Sigma)} \mathcal{Z} = T_x \mathbb{R}^m \times T_\mu \mathbb{R}^n \times T_\Sigma \mathbb{S}_{++}^n$ and with the standard product Riemannian metric (3.3). The result then follows. We note that if we let $\mathbb{D}((x_1, \mu_1, \Sigma_1), (x_2, \mu_2, \Sigma_2))$ denote the distance function corresponding to the Riemannian metric $\langle \cdot, \cdot \rangle_z$ on \mathcal{Z} , then its square $\mathbb{D}((x_1, \mu_1, \Sigma_1), (x_2, \mu_2, \Sigma_2))^2$ is the sum of the square of the distance function w.r.t. standard metric $\langle \cdot, \cdot \rangle$ on \mathbb{R}^m , the square of the distance function w.r.t. standard metric $\langle \cdot, \cdot \rangle$ on \mathbb{R}^n , and the square of the distance function w.r.t. metric $\langle \cdot, \cdot \rangle_\Sigma$ on \mathbb{S}_{++}^n . As a result and by Proposition 9, we have $\mathbb{D}((x_1, \mu_1, \Sigma_1), (x_2, \mu_2, \Sigma_2))^2 = \|x_1 - x_2\|_2^2 + \|\mu_1 - \mu_2\|_2^2 + \mathbb{B}(\Sigma_1, \Sigma_2)^2$. So, \mathbb{D} is the same as d . \square

For Lemma 4

Proof of Lemma 4. Let us express $\tilde{\nabla}_d\varphi(z) = (\Phi_1(z), \Phi_2(z), \Phi_3(z))$ with $\Phi_1(z) \in \mathbb{R}^m$, $\Phi_2(z) \in \mathbb{R}^n$ and $\Phi_3(z) \in \mathbb{S}^n$. Then by using the definition of Riemannian metric $\langle \cdot, \cdot \rangle_z$ in (3.3), we can rewrite equation (A.5) as

$$\langle \Phi_1(z), v \rangle + \langle \Phi_2(z), w \rangle + \left\langle \frac{1}{2}L_\Sigma[\Phi_3(z)], V \right\rangle = \langle \nabla\varphi(z), (v, w, V) \rangle.$$

This is equivalent to

$$\langle \Phi_1(z), v \rangle + \langle \Phi_2(z), w \rangle + \left\langle \frac{1}{2}L_\Sigma[\Phi_3(z)], V \right\rangle = \langle \nabla_x\varphi(z), v \rangle + \langle \nabla_\mu\varphi(z), w \rangle + \langle \nabla_\Sigma\varphi(z), V \rangle, \quad (\text{A.6})$$

where $\nabla\varphi(z) = (\nabla_x\varphi(z), \nabla_\mu\varphi(z), \nabla_\Sigma\varphi(z))$ denotes the standard Euclidean gradient. Equation (A.6) is obviously satisfied if $\Phi_1(z) = \nabla_x\varphi(z)$, $\Phi_2(z) = \nabla_\mu\varphi(z)$, and $L_\Sigma[\Phi_3(z)] = 2\nabla_\Sigma\varphi(z)$. By the definition of operator L_Σ right after (3.2), the third identity is the same as $\Phi_3(z) = 2[\nabla_\Sigma\varphi(z)]\Sigma + 2\Sigma[\nabla_\Sigma\varphi(z)]$. Due to uniqueness of the gradient, we therefore infer that $\tilde{\nabla}_d\varphi(z)$ is given by the formula:

$$\tilde{\nabla}_d\varphi(z) = \left(\nabla_x\varphi(z), \nabla_\mu\varphi(z), 2[\nabla_\Sigma\varphi(z)]\Sigma + 2\Sigma[\nabla_\Sigma\varphi(z)] \right).$$

This completes the proof. \square

In this paper, the optimal transport metric between any two distributions $\rho_0, \rho_1 \in \mathcal{P}(\mathcal{Z})$ is defined by

$$\mathbb{W}(\rho_0, \rho_1)^2 := \inf_{\pi \in \Pi(\rho_0, \rho_1)} \iint_{\mathcal{Z} \times \mathcal{Z}} d(z_0, z_1)^2 \pi(dz_0, dz_1), \quad (\text{A.7})$$

where $\Pi(\rho_0, \rho_1)$ is the set of all probability distributions on $\mathcal{Z} \times \mathcal{Z}$ whose marginals are ρ_0 and ρ_1 , respectively.

A.3 Proofs and Results related to Section 4

The maximum mean discrepancy (MMD) between a distribution $\rho \in \mathcal{P}(\mathcal{Z})$ and the target distribution ϱ is defined as

$$\text{MMD}(\rho, \varrho) := \sup_{f \in \mathcal{H}: \|f\|_{\mathcal{H}} \leq 1} \left\{ \int_{\mathcal{Z}} f(z) \rho(dz) - \int_{\mathcal{Z}} f(z) \varrho(dz) \right\}.$$

It is well-known that the MMD admits the following closed-form formula [Gretton *et al.*, 2012, Lemmas 4 and 6].

Lemma 10. *We have $\text{MMD}(\rho, \varrho) = \|\mathbf{m}_\rho - \mathbf{m}_\varrho\|_{\mathcal{H}}$. As a consequence,*

$$\text{MMD}(\rho, \varrho)^2 = \int_{\mathcal{Z}} \int_{\mathcal{Z}} k(z, w) \rho(dz) \rho(dw) - 2 \int_{\mathcal{Z}} \mathbf{m}_\varrho(z) \rho(dz) + \|\mathbf{m}_\varrho\|_{\mathcal{H}}^2.$$

Proof of Lemma 10. For any $f \in \mathcal{H}$, we have $f(z) = \langle f, k(\cdot, z) \rangle_{\mathcal{H}}$. Therefore,

$$\int_{\mathcal{Z}} f(z) \rho(dz) = \left\langle f, \int_{\mathcal{Z}} k(\cdot, z) \rho(dz) \right\rangle_{\mathcal{H}} = \langle f, \mathbf{m}_\rho \rangle_{\mathcal{H}} \quad \text{for all } f \in \mathcal{H}. \quad (\text{A.8})$$

It follows that $\text{MMD}(\rho, \varrho) = \sup_{f \in \mathcal{H}: \|f\|_{\mathcal{H}} \leq 1} \langle f, \mathbf{m}_\rho - \mathbf{m}_\varrho \rangle_{\mathcal{H}} = \|\mathbf{m}_\rho - \mathbf{m}_\varrho\|_{\mathcal{H}}$. Using this closed-form formula and identity (A.8), we also obtain

$$\begin{aligned} \text{MMD}(\rho, \varrho)^2 &= \|\mathbf{m}_\rho - \mathbf{m}_\varrho\|_{\mathcal{H}}^2 = \langle \mathbf{m}_\rho, \mathbf{m}_\rho \rangle_{\mathcal{H}} - 2\langle \mathbf{m}_\rho, \mathbf{m}_\varrho \rangle_{\mathcal{H}} + \langle \mathbf{m}_\varrho, \mathbf{m}_\varrho \rangle_{\mathcal{H}} \\ &= \int_{\mathcal{Z}} \mathbf{m}_\rho(z) \rho(dz) - 2 \int_{\mathcal{Z}} \mathbf{m}_\varrho(z) \rho(dz) + \|\mathbf{m}_\varrho\|_{\mathcal{H}}^2 \\ &= \iint_{\mathcal{Z}} k(z, w) \rho(dz) \rho(dw) - 2 \int_{\mathcal{Z}} \mathbf{m}_\varrho(z) \rho(dz) + \|\mathbf{m}_\varrho\|_{\mathcal{H}}^2. \end{aligned}$$

This completes the proof. \square

For Lemma 5

Proof of Lemma 5. We recall that $\text{grad } \mathcal{F}[\rho]$ is defined as the unique element in $T_\rho \mathcal{P}(\mathcal{Z})$ satisfying

$$g_\rho \left(\text{grad } \mathcal{F}[\rho], \partial_t \rho_t|_{t=0} \right) = \frac{d}{dt} \Big|_{t=0} \mathcal{F}[\rho_t]$$

for every differentiable curve $t \mapsto \rho_t \in \mathcal{P}(\mathcal{Z})$ passing through ρ at $t = 0$. Let $t \mapsto \rho_t \in \mathcal{P}(\mathcal{Z})$ be such a curve. Then since $\partial_t \rho_t|_{t=0} \in T_\rho \mathcal{P}(\mathcal{Z})$, we can write $\partial_t \rho_t|_{t=0} = -\text{div}_d(\rho \tilde{\nabla}_d \varphi)$ for some differentiable function φ on \mathcal{Z} . Then by using Lemma 10 and $k(z, w) = k(w, z)$ we have

$$\begin{aligned} \frac{d}{dt} \Big|_{t=0} \mathcal{F}[\rho_t] &= \frac{1}{2} \frac{d}{dt} \Big|_{t=0} \left[\iint k(z, w) \rho_t(dz) \rho_t(dw) - 2 \int \mathbf{m}_\varrho(z) \rho_t(dz) \right] \\ &= \frac{1}{2} \iint k(z, w) \partial_t \rho_t|_{t=0}(dz) \rho(dw) + \frac{1}{2} \iint k(z, w) \partial_t \rho_t|_{t=0}(dw) \rho(dz) \\ &\quad - \int \mathbf{m}_\varrho(z) \partial_t \rho_t|_{t=0}(dz) \\ &= - \int_{\mathcal{Z}} \int_{\mathcal{Z}} k(z, w) \text{div}_d(\rho \tilde{\nabla}_d \varphi)(dz) \rho(dw) + \int_{\mathcal{Z}} \mathbf{m}_\varrho(z) \text{div}_d(\rho \tilde{\nabla}_d \varphi)(dz). \end{aligned}$$

Let $\tilde{\nabla}_d^1 k(z, w)$ denote the gradient $\tilde{\nabla}_d$ of the function $z \mapsto k(z, w)$. It then follows from the definition of the divergence operator $\text{div}_d(\rho \tilde{\nabla}_d \varphi)$ at the end of Section 3.1 that

$$\begin{aligned} \frac{d}{dt} \Big|_{t=0} \mathcal{F}[\rho_t] &= \int_{\mathcal{Z}} \int_{\mathcal{Z}} \langle \tilde{\nabla}_d^1 k(z, w), \tilde{\nabla}_d \varphi(z) \rangle_z \rho(dz) \rho(dw) - \int_{\mathcal{Z}} \langle \tilde{\nabla}_d \mathbf{m}_\varrho(z), \tilde{\nabla}_d \varphi(z) \rangle_z \rho(dz) \\ &= \int \left[\left\langle \int \tilde{\nabla}_d^1 k(z, w) \rho(dw), \tilde{\nabla}_d \varphi(z) \right\rangle_z \right] \rho(dz) - \int_{\mathcal{Z}} \langle \tilde{\nabla}_d \mathbf{m}_\varrho(z), \tilde{\nabla}_d \varphi(z) \rangle_z \rho(dz) \\ &= \int \left[\left\langle \tilde{\nabla}_d \int k(z, w) \rho(dw), \tilde{\nabla}_d \varphi(z) \right\rangle_z \right] \rho(dz) - \int_{\mathcal{Z}} \langle \tilde{\nabla}_d \mathbf{m}_\varrho(z), \tilde{\nabla}_d \varphi(z) \rangle_z \rho(dz) \\ &= \int_{\mathcal{Z}} \langle \tilde{\nabla}_d [\mathbf{m}_\rho - \mathbf{m}_\varrho](z), \tilde{\nabla}_d \varphi(z) \rangle_z \rho(dz). \end{aligned}$$

By the definition of the Riemannian metric tensor g_ρ given in (A.3) and due to $\partial_t \rho_t|_{t=0} = -\text{div}_d(\rho \tilde{\nabla}_d \varphi)$, we thus obtain

$$\begin{aligned} \frac{d}{dt} \Big|_{t=0} \mathcal{F}[\rho_t] &= g_\rho \left(-\text{div}_d(\rho \tilde{\nabla}_d [\mathbf{m}_\rho - \mathbf{m}_\varrho]), -\text{div}_d(\rho \tilde{\nabla}_d \varphi) \right) \\ &= g_\rho \left(-\text{div}_d(\rho \tilde{\nabla}_d [\mathbf{m}_\rho - \mathbf{m}_\varrho]), \partial_t \rho_t|_{t=0} \right). \end{aligned}$$

Therefore, we infer that $\text{grad } \mathcal{F}[\rho] = -\text{div}_d(\rho \tilde{\nabla}_d [\mathbf{m}_\rho - \mathbf{m}_\varrho])$ as desired. \square

For Proposition 6

Proof of Proposition 6. The proof is similar to that of Lemma 5 and with the same notation for $\tilde{\nabla}_d^1 k(z, w)$. Indeed, by the same computation at the beginning of the proof of Lemma 5 we have

$$\begin{aligned} \frac{d}{dt} \mathcal{F}[\rho_t] &= \frac{1}{2} \iint k(z, w) \partial_t \rho_t(dz) \rho_t(dw) + \frac{1}{2} \iint k(z, w) \partial_t \rho_t(dw) \rho_t(dz) - \int \mathbf{m}_\varrho(z) \partial_t \rho_t(dz) \\ &= \iint k(z, w) \partial_t \rho_t(dz) \rho_t(dw) - \int \mathbf{m}_\varrho(z) \partial_t \rho_t(dz). \end{aligned}$$

This together with the gradient flow equation (4.1) gives

$$\begin{aligned} \frac{d}{dt} \mathcal{F}[\rho_t] &= \int_{\mathcal{Z}} \int_{\mathcal{Z}} k(z, w) \text{div}_d(\rho_t \tilde{\nabla}_d [\mathbf{m}_{\rho_t} - \mathbf{m}_\varrho])(dz) \rho_t(dw) \\ &\quad - \int_{\mathcal{Z}} \mathbf{m}_\varrho(z) \text{div}_d(\rho_t \tilde{\nabla}_d [\mathbf{m}_{\rho_t} - \mathbf{m}_\varrho])(dz). \end{aligned}$$

Using the definition of the divergence operator div_d at the end of Section 3.1, we further obtain

$$\begin{aligned}
\frac{d}{dt} \mathcal{F}[\rho_t] &= - \int_{\mathcal{Z}} \int_{\mathcal{Z}} \langle \tilde{\nabla}_d^1 k(z, w), \tilde{\nabla}_d[\mathbf{m}_{\rho_t} - \mathbf{m}_{\varrho}](z) \rangle_z \rho_t(dz) \rho_t(dw) \\
&\quad + \int_{\mathcal{Z}} \langle \tilde{\nabla}_d \mathbf{m}_{\varrho}(z), \tilde{\nabla}_d[\mathbf{m}_{\rho_t} - \mathbf{m}_{\varrho}](z) \rangle_z \rho_t(dz) \\
&= - \int_{\mathcal{Z}} \left[\left\langle \int \tilde{\nabla}_d^1 k(z, w) \rho_t(dw), \tilde{\nabla}_d[\mathbf{m}_{\rho_t} - \mathbf{m}_{\varrho}](z) \right\rangle_z \right] \rho_t(dz) \\
&\quad + \int_{\mathcal{Z}} \langle \tilde{\nabla}_d \mathbf{m}_{\varrho}(z), \tilde{\nabla}_d[\mathbf{m}_{\rho_t} - \mathbf{m}_{\varrho}](z) \rangle_z \rho_t(dz) \\
&= - \int_{\mathcal{Z}} \langle \tilde{\nabla}_d \mathbf{m}_{\rho_t}(z), \tilde{\nabla}_d[\mathbf{m}_{\rho_t} - \mathbf{m}_{\varrho}](z) \rangle_z \rho_t(dz) \\
&\quad + \int_{\mathcal{Z}} \langle \tilde{\nabla}_d \mathbf{m}_{\varrho}(z), \tilde{\nabla}_d[\mathbf{m}_{\rho_t} - \mathbf{m}_{\varrho}](z) \rangle_z \rho_t(dz) \\
&= - \int_{\mathcal{Z}} \|\tilde{\nabla}_d[\mathbf{m}_{\rho_t} - \mathbf{m}_{\varrho}](z)\|_z^2 \rho_t(dz).
\end{aligned}$$

This yields the desired result. \square

For Lemma 7

Proof of Lemma 7. From the formula for $\exp_z(\varepsilon\Phi(z))$ given at the beginning of Section 4.1, we observe that

$$\begin{aligned}
\left. \frac{d}{d\varepsilon} \right|_{\varepsilon=0} \exp_z(\varepsilon\Phi(z)) &= \left(\Phi_1(z), \Phi_2(z), L_{\Sigma}[\Phi_3(z)] \Sigma + \Sigma L_{\Sigma}[\Phi_3(z)] \right) \\
&= \left(\Phi_1(z), \Phi_2(z), \Phi_3(z) \right) = \Phi(z),
\end{aligned} \tag{A.9}$$

where the second equality is due to the definition of $L_{\Sigma}[V]$ given at the beginning of Section 3.1.

We obtain from Lemma 10 that

$$\begin{aligned}
&\text{MMD}(\exp(\varepsilon\Phi)_{\#} \rho^{\tau}, \varrho)^2 \\
&= \iint k(z, w) \exp(\varepsilon\Phi)_{\#} \rho^{\tau}(dz) \exp(\varepsilon\Phi)_{\#} \rho^{\tau}(dw) - 2 \int \mathbf{m}_{\varrho}(z) \exp(\varepsilon\Phi)_{\#} \rho^{\tau}(dz) + \|\mathbf{m}_{\varrho}\|_{\mathcal{H}}^2 \\
&= \iint k\left(\exp_z(\varepsilon\Phi(z)), \exp_w(\varepsilon\Phi(w))\right) \rho^{\tau}(dz) \rho^{\tau}(dw) - 2 \int \mathbf{m}_{\varrho}\left(\exp_z(\varepsilon\Phi(z))\right) \rho^{\tau}(dz) + \|\mathbf{m}_{\varrho}\|_{\mathcal{H}}^2.
\end{aligned}$$

Moreover, we have

$$\begin{aligned}
&\iint \left. \frac{d}{d\varepsilon} \right|_{\varepsilon=0} \left[k(\exp_z(\varepsilon\Phi(z)), \exp_w(\varepsilon\Phi(w))) \right] \rho^{\tau}(dz) \rho^{\tau}(dw) \\
&= \iint \left\{ \left. \frac{d}{d\varepsilon} \right|_{\varepsilon=0} \left[k(\exp_z(\varepsilon\Phi(z)), w) \right] + \left. \frac{d}{d\varepsilon} \right|_{\varepsilon=0} \left[k(z, \exp_w(\varepsilon\Phi(w))) \right] \right\} \rho^{\tau}(dz) \rho^{\tau}(dw) \\
&= \int \left. \frac{d}{d\varepsilon} \right|_{\varepsilon=0} \left[\int k(\exp_z(\varepsilon\Phi(z)), w) \rho^{\tau}(dw) \right] \rho^{\tau}(dz) + \int \left. \frac{d}{d\varepsilon} \right|_{\varepsilon=0} \left[\int k(z, \exp_w(\varepsilon\Phi(w))) \rho^{\tau}(dz) \right] \rho^{\tau}(dw) \\
&= \int \left. \frac{d}{d\varepsilon} \right|_{\varepsilon=0} \left[\mathbf{m}_{\rho^{\tau}}(\exp_z(\varepsilon\Phi(z))) \right] \rho^{\tau}(dz) + \int \left. \frac{d}{d\varepsilon} \right|_{\varepsilon=0} \left[\mathbf{m}_{\rho^{\tau}}(\exp_w(\varepsilon\Phi(w))) \right] \rho^{\tau}(dw) \\
&= 2 \int \left. \frac{d}{d\varepsilon} \right|_{\varepsilon=0} \left[\mathbf{m}_{\rho^{\tau}}(\exp_z(\varepsilon\Phi(z))) \right] \rho^{\tau}(dz).
\end{aligned}$$

Thus, it follows that

$$\begin{aligned}
&\left. \frac{d}{d\varepsilon} \right|_{\varepsilon=0} \text{MMD}(\exp(\varepsilon\Phi)_{\#} \rho^{\tau}, \varrho)^2 \\
&= 2 \int \left. \frac{d}{d\varepsilon} \right|_{\varepsilon=0} \left[\mathbf{m}_{\rho^{\tau}}(\exp_z(\varepsilon\Phi(z))) \right] \rho^{\tau}(dz) - 2 \int \left. \frac{d}{d\varepsilon} \right|_{\varepsilon=0} \left[\mathbf{m}_{\varrho}(\exp_z(\varepsilon\Phi(z))) \right] \rho^{\tau}(dz) \\
&= 2 \int D[\mathbf{m}_{\rho^{\tau}} - \mathbf{m}_{\varrho}]_z \left(\left. \frac{d}{d\varepsilon} \right|_{\varepsilon=0} \exp_z(\varepsilon\Phi(z)) \right) \rho^{\tau}(dz)
\end{aligned}$$

with $D\varphi_z(w, v, V)$ denoting the standard directional derivative of φ at z in the direction (w, v, V) . Using the definition of \mathcal{F} together with (A.9) and the definition of gradient $\tilde{\nabla}_d$ in (A.5), we obtain

$$\begin{aligned} \frac{d}{d\varepsilon} \Big|_{\varepsilon=0} \mathcal{F}[\exp(\varepsilon\Phi)_{\#}\rho^\tau] &= \int D[\mathbf{m}_{\rho^\tau} - \mathbf{m}_\varrho]_z(\Phi(z)) \rho^\tau(dz) \\ &= \int \langle \tilde{\nabla}_d[\mathbf{m}_{\rho^\tau} - \mathbf{m}_\varrho](z), \Phi(z) \rangle_z \rho^\tau(dz). \end{aligned} \quad (\text{A.10})$$

This yields the first conclusion of the lemma.

Now let $\hat{\Phi}^\tau := \frac{\Phi^\tau}{\|\Phi^\tau\|_{\mathbb{L}^2(\rho^\tau)}}$ be the unit vector field in the direction of $\Phi^\tau := -\tilde{\nabla}_d[\mathbf{m}_{\rho^\tau} - \mathbf{m}_\varrho]$. Then by (A.10), we have

$$\frac{d}{d\varepsilon} \Big|_{\varepsilon=0} \mathcal{F}[\exp(\varepsilon\hat{\Phi}^\tau)_{\#}\rho^\tau] = -\|\Phi^\tau\|_{\mathbb{L}^2(\rho^\tau)}^{-1} \int \|\Phi^\tau(z)\|_z^2 \rho^\tau(dz) = -\|\Phi^\tau\|_{\mathbb{L}^2(\rho^\tau)} \leq 0.$$

On the other hand, for any unit direction Φ in $\mathbb{L}^2(\rho^\tau)$ we obtain from (A.10) and Hölder inequality that

$$\begin{aligned} \left| \frac{d}{d\varepsilon} \Big|_{\varepsilon=0} \mathcal{F}[\exp(\varepsilon\Phi)_{\#}\rho^\tau] \right| &\leq \int \|\Phi^\tau(z)\|_z \|\Phi(z)\|_z \rho^\tau(dz) \\ &\leq \left(\int \|\Phi^\tau(z)\|_z^2 \rho^\tau(dz) \right)^{\frac{1}{2}} \left(\int \|\Phi(z)\|_z^2 \rho^\tau(dz) \right)^{\frac{1}{2}} = \|\Phi^\tau\|_{\mathbb{L}^2(\rho^\tau)}. \end{aligned}$$

Therefore, we conclude further that

$$\frac{d}{d\varepsilon} \Big|_{\varepsilon=0} \mathcal{F}[\exp(\varepsilon\hat{\Phi}^\tau)_{\#}\rho^\tau] \leq \frac{d}{d\varepsilon} \Big|_{\varepsilon=0} \mathcal{F}[\exp(\varepsilon\Phi)_{\#}\rho^\tau]$$

for any unit direction Φ in $\mathbb{L}^2(\rho^\tau)$. These give the last conclusion of the lemma. \square

Definition 11 (Lipschitz-gradient kernel). *Let $L > 0$. A differentiable kernel k on \mathcal{Z} is called a Lipschitz-gradient kernel with constant L if there exists a number $\varepsilon_0 \in (0, 1)$ such that*

$$\begin{aligned} &\left| k(\exp_z(\varepsilon\Phi(z)), \exp_w(\delta\Phi(w))) - k(z, w) - [\langle \tilde{\nabla}_d^1 k(z, w), \varepsilon\Phi(z) \rangle_z + \langle \tilde{\nabla}_d^2 k(z, w), \delta\Phi(w) \rangle_w] \right| \\ &\leq L \left[\|\varepsilon\Phi(z)\|_z^2 + \|\delta\Phi(w)\|_w^2 \right] \end{aligned} \quad (\text{A.11})$$

for every $\varepsilon, \delta \in [0, \varepsilon_0]$ and every bounded vector field $\Phi : \mathcal{Z} \rightarrow \mathbb{R}^m \times \mathbb{R}^n \times \mathbb{S}^n$. Hereafter, $\tilde{\nabla}_d^1 k(z, w)$ and $\tilde{\nabla}_d^2 k(z, w)$ denote respectively the gradient $\tilde{\nabla}_d$ of the function $z \mapsto k(z, w)$ and the function $w \mapsto k(z, w)$.

Remark 12. *The right hand side of condition (A.11) can be expressed in terms of the d distance as*

$$d(\exp_z(\varepsilon\Phi(z)), z)^2 + d(\exp_w(\delta\Phi(w)), w)^2.$$

Thus condition (A.11) can be interpreted as the gradient $\tilde{\nabla}_d k$ is Lipschitz w.r.t. the distance d .

Condition (A.11) is motivated by the following observation in the Euclidean space. Assume that $G : \mathbb{R}^d \times \mathbb{R}^d \rightarrow \mathbb{R}$ is a differentiable function such that its Euclidean gradient $\nabla G(z, w) := (\nabla^1 G(z, w), \nabla^2 G(z, w))$ satisfies the standard Lipschitz condition

$$\|\nabla G(z_1, w_1) - \nabla G(z_2, w_2)\|_2 \leq L \|(z_1, w_1) - (z_2, w_2)\|_2 \quad \forall (z_1, w_1), (z_2, w_2) \in \mathbb{R}^d \times \mathbb{R}^d.$$

Then for any point $(z, w) \in \mathbb{R}^d \times \mathbb{R}^d$ and any tangent vector $(u, v) \in \mathbb{R}^d \times \mathbb{R}^d$, we have by using the mean value theorem that $G(z + u, w + v) - G(z, w) = \langle \nabla G(z_0, w_0), (u, v) \rangle$ for some point (z_0, w_0) in the line segment in $\mathbb{R}^d \times \mathbb{R}^d$ connecting the points (z, w) and $(z + u, w + v)$. As a consequence, we obtain

$$\begin{aligned} &\left| G(z + u, w + v) - G(z, w) - [\langle \nabla^1 G(z, w), u \rangle + \langle \nabla^2 G(z, w), v \rangle] \right| \\ &= \left| \langle \nabla G(z_0, w_0), (u, v) \rangle - \langle \nabla G(z, w), (u, v) \rangle \right| \\ &= \left| \langle \nabla G(z_0, w_0) - \nabla G(z, w), (u, v) \rangle \right| \leq \|\nabla G(z_0, w_0) - \nabla G(z, w)\|_2 \|(u, v)\|_2. \end{aligned}$$

Then we can use the Lipschitz condition for ∇G to imply further that

$$\begin{aligned} &\left| G(z + u, w + v) - G(z, w) - [\langle \nabla^1 G(z, w), u \rangle + \langle \nabla^2 G(z, w), v \rangle] \right| \\ &\leq L \|(z_0, w_0) - (z, w)\|_2 \|(u, v)\|_2 \leq L \|(u, v)\|_2^2, \end{aligned}$$

which is the same as

$$\left| G(z + u, w + v) - G(z, w) - [\langle \nabla^1 G(z, w), u \rangle + \langle \nabla^2 G(z, w), v \rangle] \right| \leq L[\|u\|_2^2 + \|v\|_2^2].$$

Condition (A.11) is the Riemannian version of this last inequality for the Euclidean space, which is a consequence of the standard Lipschitz condition for the gradient.

Bounded Hessian kernels are Lipschitz-gradient. The following lemma gives a sufficient condition for a kernel to be Lipschitz-gradient.

Lemma 13. *Let k be a positive definite kernel such that its Hessian w.r.t. distance d is bounded. Then k is a Lipschitz-gradient kernel.*

Proof of Lemma 13. Let $H_d^1 k(z, w)$ and $H_d^2 k(z, w)$ denote respectively the Hessian w.r.t. distance d of the function $z \mapsto k(z, w)$ and the function $w \mapsto k(z, w)$. Let $\varepsilon, \delta > 0$, and $\Phi : \mathcal{Z} \rightarrow \mathbb{R}^m \times \mathbb{R}^n \times \mathbb{S}^n$ be a bounded vector field. Define $\gamma_z(t) := \exp_z(t\Phi(z))$ and $\theta_w(t) := \exp_w(\frac{\delta}{\varepsilon}t\Phi(w))$ for $t \in [0, \varepsilon]$. Then we have

$$\begin{aligned} k(\exp_z(\varepsilon\Phi(z)), \exp_w(\delta\Phi(w))) - k(z, w) &= \int_0^\varepsilon \frac{d}{dt} [k(\gamma_z(t), \theta_w(t))] dt \\ &= \int_0^\varepsilon \left[\langle \tilde{\nabla}_d^1 k(\gamma_z(t), \theta_w(t)), \dot{\gamma}_z(t) \rangle_{\gamma_z(t)} + \langle \tilde{\nabla}_d^2 k(\gamma_z(t), \theta_w(t)), \dot{\theta}_w(t) \rangle_{\theta_w(t)} \right] dt. \end{aligned}$$

This together with the facts that $\dot{\gamma}_z(0) = \Phi(z)$ and $\dot{\theta}_w(0) = \frac{\delta}{\varepsilon}\Phi(w)$ yields

$$\begin{aligned} A &:= k(\exp_z(\varepsilon\Phi(z)), \exp_w(\delta\Phi(w))) - k(z, w) - \left[\langle \tilde{\nabla}_d^1 k(z, w), \varepsilon\Phi(z) \rangle_z + \langle \tilde{\nabla}_d^2 k(z, w), \delta\Phi(w) \rangle_w \right] \\ &= \int_0^\varepsilon \left[\langle \tilde{\nabla}_d^1 k(\gamma_z(t), \theta_w(t)), \dot{\gamma}_z(t) \rangle_{\gamma_z(t)} - \langle \tilde{\nabla}_d^1 k(\gamma_z(0), \theta_w(0)), \dot{\gamma}_z(0) \rangle_{\gamma_z(0)} \right] dt \\ &\quad + \int_0^\varepsilon \left[\langle \tilde{\nabla}_d^2 k(\gamma_z(t), \theta_w(t)), \dot{\theta}_w(t) \rangle_{\theta_w(t)} - \langle \tilde{\nabla}_d^2 k(\gamma_z(0), \theta_w(0)), \dot{\theta}_w(0) \rangle_{\theta_w(0)} \right] dt \\ &= \int_0^\varepsilon \int_0^t \frac{d}{ds} \left[\langle \tilde{\nabla}_d^1 k(\gamma_z(s), \theta_w(s)), \dot{\gamma}_z(s) \rangle_{\gamma_z(s)} \right] ds dt \\ &\quad + \int_0^\varepsilon \int_0^t \frac{d}{ds} \left[\langle \tilde{\nabla}_d^2 k(\gamma_z(s), \theta_w(s)), \dot{\theta}_w(s) \rangle_{\theta_w(s)} \right] ds dt \\ &= \int_0^\varepsilon \int_0^t \left[\langle H_d^1 k(\gamma_z(s), \theta_w(s)) \dot{\gamma}_z(s), \dot{\gamma}_z(s) \rangle_{\gamma_z(s)} + \langle \tilde{\nabla}_d^1 k(\gamma_z(s), \theta_w(s)), \ddot{\gamma}_z(s) \rangle_{\gamma_z(s)} \right] ds dt \\ &\quad + \int_0^\varepsilon \int_0^t \left[\langle H_d^2 k(\gamma_z(s), \theta_w(s)) \dot{\theta}_w(s), \dot{\theta}_w(s) \rangle_{\theta_w(s)} + \langle \tilde{\nabla}_d^2 k(\gamma_z(s), \theta_w(s)), \ddot{\theta}_w(s) \rangle_{\theta_w(s)} \right] ds dt. \end{aligned}$$

Since the curve $s \mapsto \gamma_z(s)$ is a geodesic, its acceleration $\ddot{\gamma}_z(s)$ is orthogonal to \mathcal{Z} (that is, $\ddot{\gamma}_z(s)$ is orthogonal to every tangent vector in $T_z\mathcal{Z}$). This implies that $\langle \tilde{\nabla}_d^1 k(\gamma_z(s), \theta_w(s)), \ddot{\gamma}_z(s) \rangle_{\gamma_z(s)} = 0$. Likewise, we also have $\langle \tilde{\nabla}_d^2 k(\gamma_z(s), \theta_w(s)), \ddot{\theta}_w(s) \rangle_{\theta_w(s)} = 0$. Thanks to these, we deduce from the above identity that

$$\begin{aligned} A &= \int_0^\varepsilon \int_0^t \langle H_d^1 k(\gamma_z(s), \theta_w(s)) \dot{\gamma}_z(s), \dot{\gamma}_z(s) \rangle_{\gamma_z(s)} ds dt \\ &\quad + \int_0^\varepsilon \int_0^t \langle H_d^2 k(\gamma_z(s), \theta_w(s)) \dot{\theta}_w(s), \dot{\theta}_w(s) \rangle_{\theta_w(s)} ds dt. \end{aligned}$$

By using the assumption that the Hessians H_d^1 and H_d^2 are bounded, we then obtain

$$|A| \leq M \int_0^\varepsilon \int_0^t \left[\|\dot{\gamma}_z(s)\|_{\gamma_z(s)}^2 + \|\dot{\theta}_w(s)\|_{\theta_w(s)}^2 \right] ds dt,$$

where M is the sup norm of the Hessian of k . But as $\gamma_z(s)$ and $\theta_w(s)$ are geodesic, they have constant speeds. Therefore, $\|\dot{\gamma}_z(s)\|_{\gamma_z(s)} = \|\dot{\gamma}_z(0)\|_{\gamma_z(0)} = \|\Phi(z)\|_z$ and $\|\dot{\theta}_w(s)\|_{\theta_w(s)} = \|\dot{\theta}_w(0)\|_{\theta_w(0)} = \|\frac{\delta}{\varepsilon}\Phi(w)\|_w$. Using these, we infer further that

$$|A| \leq M \int_0^\varepsilon \int_0^t \left[\|\Phi(z)\|_z^2 + \left(\frac{\delta}{\varepsilon}\right)^2 \|\Phi(w)\|_w^2 \right] ds dt = \frac{M}{2} \left[\|\varepsilon\Phi(z)\|_z^2 + \|\delta\Phi(w)\|_w^2 \right].$$

According to Definition 11, we thus conclude that k is a Lipschitz-gradient kernel with constant $M/2$. \square

Quantified estimate of decrease for the Riemannian forward Euler scheme (4.2). The next result quantifies the amount that the value of \mathcal{F} decreases after each iteration.

Proposition 14 (Quantified estimate of decrease). *Suppose that k is a Lipschitz-gradient kernel with constant L . Then for $\rho^{\tau+1}$ given by (4.2) with $s_\tau \in (0, \varepsilon_0]$, we have*

$$\mathcal{F}[\rho^{\tau+1}] - \mathcal{F}[\rho^\tau] \leq -s_\tau(1 - 2Ls_\tau) \int_{\mathcal{Z}} \|\tilde{\nabla}_d[\mathbf{m}_{\rho^\tau} - \mathbf{m}_\theta](z)\|_z^2 \rho^\tau(dz).$$

Proof of Proposition 14. Let $\Phi^\tau := -\tilde{\nabla}_d[\mathbf{m}_{\rho^\tau} - \mathbf{m}_\varrho]$. Then from the computation at the beginning of the proof of Lemma 7 and by using Lemma 10, we obtain

$$\begin{aligned} \mathcal{F}[\rho^{\tau+1}] - \mathcal{F}[\rho^\tau] &= \frac{1}{2} [\text{MMD}(\exp(s_\tau \Phi^\tau)_{\#} \rho^\tau, \varrho)^2 - \text{MMD}(\rho^\tau, \varrho)^2] \\ &= \frac{1}{2} \iint \left\{ k\left(\exp_z(s_\tau \Phi^\tau(z)), \exp_w(s_\tau \Phi^\tau(w))\right) - k(z, w) \right\} \rho^\tau(dz) \rho^\tau(dw) \\ &\quad - \iint \left\{ k\left(\exp_z(s_\tau \Phi^\tau(z)), w\right) - k(z, w) \right\} \rho^\tau(dz) \varrho(dw). \end{aligned}$$

Moreover, we have

$$\begin{aligned} &\int \langle \tilde{\nabla}_d[\mathbf{m}_{\rho^\tau} - \mathbf{m}_\varrho](z), \Phi^\tau(z) \rangle_z \rho^\tau(dz) \\ &= \iint \langle \tilde{\nabla}_d^1 k(z, w), \Phi^\tau(z) \rangle_z \rho^\tau(dz) \rho^\tau(dw) - \iint \langle \tilde{\nabla}_d^1 k(z, w), \Phi^\tau(z) \rangle_z \rho^\tau(dz) \varrho(dw) \\ &= \frac{1}{2} \left[\iint \langle \tilde{\nabla}_d^1 k(z, w), \Phi^\tau(z) \rangle_z \rho^\tau(dz) \rho^\tau(dw) + \iint \langle \tilde{\nabla}_d^2 k(z, w), \Phi^\tau(w) \rangle_w \rho^\tau(dz) \rho^\tau(dw) \right] \\ &\quad - \iint \langle \tilde{\nabla}_d^1 k(z, w), \Phi^\tau(z) \rangle_z \rho^\tau(dz) \varrho(dw), \end{aligned}$$

where the last equality is due to the symmetry of k and relation (3.6). Here $\tilde{\nabla}_d^1 k(z, w)$ and $\tilde{\nabla}_d^2 k(z, w)$ respectively denote the gradient $\tilde{\nabla}_d$ of the function $z \mapsto k(z, w)$ and $w \mapsto k(z, w)$. Therefore, it follows that

$$\begin{aligned} \mathcal{F}[\rho^{\tau+1}] - \mathcal{F}[\rho^\tau] - s_\tau \int \langle \tilde{\nabla}_d[\mathbf{m}_{\rho^\tau} - \mathbf{m}_\varrho](z), \Phi^\tau(z) \rangle_z \rho^\tau(dz) \\ &= \frac{1}{2} \iint \left\{ k\left(\exp_z(s_\tau \Phi^\tau(z)), \exp_w(s_\tau \Phi^\tau(w))\right) - k(z, w) \right. \\ &\quad \left. - \left[\langle \tilde{\nabla}_d^1 k(z, w), s_\tau \Phi^\tau(z) \rangle_z + \langle \tilde{\nabla}_d^2 k(z, w), s_\tau \Phi^\tau(w) \rangle_w \right] \right\} \rho^\tau(dz) \rho^\tau(dw) \\ &\quad - \iint \left\{ k\left(\exp_z(s_\tau \Phi^\tau(z)), w\right) - k(z, w) - \langle \tilde{\nabla}_d^1 k(z, w), s_\tau \Phi^\tau(z) \rangle_z \right\} \rho^\tau(dz) \varrho(dw). \end{aligned}$$

As $s_\tau \in (0, \varepsilon_0]$, we can now use the assumption that k is a Lipschitz-gradient kernel with constant L to obtain

$$\begin{aligned} \mathcal{F}[\rho^{\tau+1}] - \mathcal{F}[\rho^\tau] + s_\tau \int_{\mathcal{Z}} \|\Phi^\tau(z)\|_z^2 \rho^\tau(dz) \\ &\leq \frac{L}{2} \iint \left[\|s_\tau \Phi^\tau(z)\|_z^2 + \|s_\tau \Phi^\tau(w)\|_w^2 \right] \rho^\tau(dz) \rho^\tau(dw) + L \iint \|s_\tau \Phi^\tau(z)\|_z^2 \rho^\tau(dz) \varrho(dw) \\ &= 2Ls_\tau^2 \int_{\mathcal{Z}} \|\Phi^\tau(z)\|_z^2 \rho^\tau(dz). \end{aligned}$$

This gives

$$\mathcal{F}[\rho^{\tau+1}] - \mathcal{F}[\rho^\tau] \leq (-s_\tau + 2Ls_\tau^2) \int_{\mathcal{Z}} \|\Phi^\tau(z)\|_z^2 \rho^\tau(dz),$$

and the conclusion of the proposition follows. \square

Convergence guarantees. For each distribution ρ on \mathcal{Z} , let $\mathbb{K}_\rho : \mathcal{H} \rightarrow \mathcal{H}$ be the linear operator defined by $\mathbb{K}_\rho f(w_1) := \langle \tilde{\mathbb{K}}_\rho(w_1, \cdot), f(\cdot) \rangle_{\mathcal{H}}$ with $\tilde{\mathbb{K}}_\rho : \mathcal{Z} \times \mathcal{Z} \rightarrow \mathbb{R}$ being given by

$$\tilde{\mathbb{K}}_\rho(w_1, w_2) = \int_{\mathcal{Z}} \langle \tilde{\nabla}_d^1 k(z, w_1), \tilde{\nabla}_d^1 k(z, w_2) \rangle_z \rho(dz) \quad \text{for } w_1, w_2 \in \mathcal{Z}.$$

The next result gives some basic properties of the operator \mathbb{K}_ρ .

Lemma 15. For a differentiable kernel k and for $\rho \in \mathcal{P}(\mathcal{Z})$, we have

- i) $\mathbb{K}_\rho f(w) = \int_{\mathcal{Z}} \langle \tilde{\nabla}_d^1 k(z, w), \tilde{\nabla}_d f(z) \rangle_z \rho(dz)$ for $f \in \mathcal{H}$.
- ii) $\langle \mathbb{K}_\rho f, g \rangle_{\mathcal{H}} = \int_{\mathcal{Z}} \langle \tilde{\nabla}_d f, \tilde{\nabla}_d g \rangle_z \rho(dz)$ for every $f, g \in \mathcal{H}$. Consequently, the operator \mathbb{K}_ρ is symmetric and positive, and hence its spectrum is contained in $[0, +\infty)$.

Proof of Lemma 15. By using the definition of the Riemannian metric $\langle \cdot, \cdot \rangle_z$ given in (3.3), it can be verified for $f \in \mathcal{H}$ that

$$\left\langle \langle \tilde{\nabla}_d^1 k(z, w), \tilde{\nabla}_d^1 k(z, \cdot) \rangle_z, f(\cdot) \right\rangle_{\mathcal{H}} = \left\langle \tilde{\nabla}_d^1 k(z, w), \langle \tilde{\nabla}_d^1 k(z, \cdot), f(\cdot) \rangle_{\mathcal{H}} \right\rangle_z.$$

As $f(z) = \langle k(z, \cdot), f(\cdot) \rangle_{\mathcal{H}}$, we moreover have $\tilde{\nabla}_d f(z) = \langle \tilde{\nabla}_d^1 k(z, \cdot), f(\cdot) \rangle_{\mathcal{H}}$. Therefore,

$$\left\langle \langle \tilde{\nabla}_d^1 k(z, w), \tilde{\nabla}_d^1 k(z, \cdot) \rangle_z, f(\cdot) \right\rangle_{\mathcal{H}} = \left\langle \tilde{\nabla}_d^1 k(z, w), \tilde{\nabla}_d f(z) \right\rangle_z. \quad (\text{A.12})$$

Using the definition of \mathbb{K}_ρ and (A.12), we obtain

$$\begin{aligned} \mathbb{K}_\rho f(w) &= \left\langle \int \langle \tilde{\nabla}_d^1 k(z, w), \tilde{\nabla}_d^1 k(z, \cdot) \rangle_z \rho(dz), f(\cdot) \right\rangle_{\mathcal{H}} \\ &= \int \left\langle \langle \tilde{\nabla}_d^1 k(z, w), \tilde{\nabla}_d^1 k(z, \cdot) \rangle_z, f(\cdot) \right\rangle_{\mathcal{H}} \rho(dz) \\ &= \int \langle \tilde{\nabla}_d^1 k(z, w), \tilde{\nabla}_d f(z) \rangle_z \rho(dz), \end{aligned}$$

which gives i). Now for $f, g \in \mathcal{H}$, we can use part i) and similar arguments leading to (A.12) to obtain

$$\begin{aligned} \langle \mathbb{K}_\rho f, g \rangle_{\mathcal{H}} &= \left\langle \int \langle \tilde{\nabla}_d^1 k(z, \cdot), \tilde{\nabla}_d f(z) \rangle_z \rho(dz), g(\cdot) \right\rangle_{\mathcal{H}} \\ &= \int \left\langle \langle \tilde{\nabla}_d^1 k(z, \cdot), \tilde{\nabla}_d f(z) \rangle_z, g(\cdot) \right\rangle_{\mathcal{H}} \rho(dz) \\ &= \int \left\langle \langle \tilde{\nabla}_d^1 k(z, \cdot), g(\cdot) \rangle_{\mathcal{H}}, \tilde{\nabla}_d f(z) \right\rangle_z \rho(dz) = \int \langle \tilde{\nabla}_d g(z), \tilde{\nabla}_d f(z) \rangle_z \rho(dz). \end{aligned}$$

This implies in particular that the operator \mathbb{K}_ρ is symmetric (i.e. $\langle \mathbb{K}_\rho f, g \rangle_{\mathcal{H}} = \langle \mathbb{K}_\rho g, f \rangle_{\mathcal{H}}$ for $f, g \in \mathcal{H}$) and positive (i.e. $\langle \mathbb{K}_\rho f, f \rangle_{\mathcal{H}} \geq 0$ for $f \in \mathcal{H}$). Since any symmetric, positive, and linear operator must have nonnegative eigenvalues, we have completed the proof. \square

Our next result gives a quantified decay rate for the objective function.

Proposition 16 (Objective value decay). *There hold:*

i) Let ρ_t be given by (4.1), and let $\lambda_t \geq 0$ be any constant satisfying

$$\langle \mathbb{K}_{\rho_t} f_t, f_t \rangle_{\mathcal{H}} \geq \lambda_t \|f_t\|_{\mathcal{H}}^2 \quad \text{with} \quad f_t := \mathbf{m}_{\rho_t} - \mathbf{m}_\varrho. \quad (\text{A.13})$$

Then $\mathcal{F}[\rho_t] \leq \mathcal{F}[\rho_0] \exp(-2 \int_0^t \lambda_s ds)$ for any $t \geq 0$. In particular, $\lim_{t \rightarrow \infty} \text{MMD}(\rho_t, \varrho) = 0$ if $\int_0^\infty \lambda_t dt = +\infty$.

ii) Let ρ^τ be given by scheme (4.2), and $\lambda_\tau \geq 0$ be any constant satisfying

$$\langle \mathbb{K}_{\rho_t} f^\tau, f^\tau \rangle_{\mathcal{H}} \geq \lambda_\tau \|f^\tau\|_{\mathcal{H}}^2 \quad \text{with} \quad f^\tau := \mathbf{m}_{\rho^\tau} - \mathbf{m}_\varrho.$$

Assume that k is a Lipschitz-gradient kernel and step size s_τ satisfies $s_\tau \lambda_\tau < 1$, then we have $\mathcal{F}[\rho^{\tau+1}] \leq \mathcal{F}[\rho^0] \exp(-\sum_{i=0}^\tau s_i \lambda_i)$ for any $\tau \geq 0$. In particular, $\lim_{\tau \rightarrow \infty} \text{MMD}(\rho^\tau, \varrho) = 0$ if $\sum_{\tau=0}^\infty s_\tau \lambda_\tau = +\infty$.

Condition $\int_0^\infty \lambda_t dt = +\infty$ guaranteeing the convergence in MMD holds true for example if $\lambda_t \geq ct^{-1}$ for some constant $c > 0$ and for large t . We note also that Condition (A.13) is satisfied if λ_t is chosen to be the minimum eigenvalue of operator \mathbb{K}_{ρ_t} . Thus Proposition 16 implies in particular that ρ_t globally converges in MMD if the minimum eigenvalue λ_t of operator \mathbb{K}_{ρ_t} satisfies the integrability condition $\int_0^\infty \lambda_t dt = +\infty$. The proof of Proposition 16 relies on the following proposition, which shows that the dynamic of the mean embedding is governed by the equation $\partial_t(\mathbf{m}_{\rho_t} - \mathbf{m}_\varrho) = -\mathbb{K}_{\rho_t}(\mathbf{m}_{\rho_t} - \mathbf{m}_\varrho)$.

Proposition 17 (Dynamic of the mean embedding). *Let $t \in [0, \infty) \mapsto \rho_t$ be the gradient flow given by equation (4.1). For each $t \geq 0$, take $f_t := \mathbf{m}_{\rho_t} - \mathbf{m}_\varrho$. Then f_t is a solution of the linear partial differential equation*

$$\partial_t f_t = -\mathbb{K}_{\rho_t} f_t \quad \text{in} \quad [0, \infty) \times \mathcal{Z}. \quad (\text{A.14})$$

Proof of Proposition 17. From the definition of the mean embedding and by using equation (4.1), we have

$$\begin{aligned} \partial_t f_t(w) &= \partial_t \mathbf{m}_{\rho_t}(w) = \partial_t \int_{\mathcal{Z}} k(z, w) \rho_t(dz) = \int_{\mathcal{Z}} k(z, w) \partial_t \rho_t(dz) \\ &= \int_{\mathcal{Z}} k(z, w) \text{div}_d(\rho_t \tilde{\nabla}_d f_t)(dz). \end{aligned}$$

Using the definition of the divergence operator div_d at the end of Section 3.1, we further obtain

$$\partial_t f_t(w) = - \int_{\mathcal{Z}} \langle \tilde{\nabla}_d^1 k(z, w), \tilde{\nabla}_d f_t(z) \rangle_z \rho_t(dz).$$

It then follows from part i) of Lemma 15 that $\partial_t f_t(w) = -\mathbb{K}_{\rho_t} f_t(w)$. This completes the proof. \square

We are now ready to present the proof of Proposition 16.

Proof of Proposition 16. Let $f_t := \mathbf{m}_{\rho_t} - \mathbf{m}_\varrho$. Then we have from Proposition 6 and part ii) of Lemma 15 that $\partial_t \|f_t\|_{\mathcal{H}}^2 = -2\langle \mathbb{K}_{\rho_t} f_t, f_t \rangle_{\mathcal{H}}$. But as

$$\langle \mathbb{K}_{\rho_t} f_t, f_t \rangle_{\mathcal{H}} \geq \lambda_t \|f_t\|_{\mathcal{H}}^2$$

by Condition A.13, we infer that $\partial_t \|f_t\|_{\mathcal{H}}^2 \leq -2\lambda_t \|f_t\|_{\mathcal{H}}^2$, and hence $\partial_t \left(\log \|f_t\|_{\mathcal{H}}^2 \right) \leq -2\lambda_t$. By integrating from 0 to t , one gets $\log \|f_t\|_{\mathcal{H}}^2 - \log \|f_0\|_{\mathcal{H}}^2 \leq -2 \int_0^t \lambda_s ds$. We next take exponential to obtain

$$\|f_t\|_{\mathcal{H}}^2 \leq \|f_0\|_{\mathcal{H}}^2 \exp \left(-2 \int_0^t \lambda_s ds \right).$$

This can be rewritten as $\mathcal{F}[\rho_t] \leq \mathcal{F}[\rho_0] \exp \left(-2 \int_0^t \lambda_s ds \right)$ for $t \geq 0$. In particular, $\mathcal{F}[\rho_t]$ (and hence $\text{MMD}(\rho_t, \varrho)$) tends to zero if $\int_0^\infty \lambda_t dt = +\infty$. This completes the proof for part i).

To prove ii), let $f^\tau := \mathbf{m}_{\rho^\tau} - \mathbf{m}_\varrho$. Notice that in contrast to the continuous case, upper indices are used for f^τ and ρ^τ in the discrete case. Then by using Proposition 14 together with part ii) of Lemma 15 and the assumption $s_\tau \in (0, \frac{1}{4L}]$ we have

$$\mathcal{F}[\rho^{\tau+1}] - \mathcal{F}[\rho^\tau] \leq -\frac{1}{2} s_\tau \langle \mathbb{K}_{\rho^\tau} f^\tau, f^\tau \rangle_{\mathcal{H}}.$$

But as $\langle \mathbb{K}_{\rho^\tau} f^\tau, f^\tau \rangle_{\mathcal{H}} \geq \lambda_\tau \|f^\tau\|_{\mathcal{H}}^2$ due to our assumption, we obtain $\mathcal{F}[\rho^{\tau+1}] - \mathcal{F}[\rho^\tau] \leq -s_\tau \lambda_\tau \mathcal{F}[\rho^\tau]$, or

$$\mathcal{F}[\rho^{\tau+1}] \leq (1 - s_\tau \lambda_\tau) \mathcal{F}[\rho^\tau]$$

for every $\tau \geq 0$. As $1 - s_\tau \lambda_\tau > 0$, it follows by iteration that $\mathcal{F}[\rho^{\tau+1}] \leq \mathcal{F}[\rho^0] \prod_{i=0}^{\tau} (1 - s_i \lambda_i)$. Due to $1 - x \leq \exp(-x)$ for

every $x \geq 0$, we infer that $\mathcal{F}[\rho^{\tau+1}] \leq \mathcal{F}[\rho^0] \exp \left(-\sum_{i=0}^{\tau} s_i \lambda_i \right)$ for $\tau \geq 0$. In particular, $\mathcal{F}[\rho^\tau]$ (and hence $\text{MMD}(\rho^\tau, \varrho)$) tends to

zero if $\sum_{\tau=0}^{\infty} s_\tau \lambda_\tau = +\infty$. □

For Proposition 8

Proof of Proposition 8. Let $h(z) := \exp_z(s_\tau \Phi^\tau(z))$ for $z \in Z$. Then $\rho^{\tau+1}$ can be expressed as

$$\rho^{\tau+1} = h_{\#} \rho^{\tau, \beta_\tau} = (h \circ f^{\beta_\tau})_{\#} (\rho^\tau \otimes g).$$

By the computation at the beginning of the proof of Lemma 7 using Lemma 10, we obtain

$$\begin{aligned} \mathcal{F}[\rho^{\tau+1}] - \mathcal{F}[\rho^\tau] &= \frac{1}{2} \left[\text{MMD} \left((h \circ f^{\beta_\tau})_{\#} (\rho^\tau \otimes g), \varrho \right)^2 - \text{MMD}(\rho^\tau, \varrho)^2 \right] \\ &= \frac{1}{2} \iiint \iiint \left\{ k \left(h(f^{\beta_\tau}(z, u)), h(f^{\beta_\tau}(w, v)) \right) - k(z, w) \right\} \rho^\tau(dz) g(du) \rho^\tau(dw) g(dv) \\ &\quad - \iiint \left\{ k \left(h(f^{\beta_\tau}(z, u)), w \right) - k(z, w) \right\} \rho^\tau(dz) g(du) \varrho(dw). \end{aligned}$$

Moreover, we have

$$\begin{aligned} I &:= \int \langle \tilde{\nabla}_d [\mathbf{m}_{\rho^\tau} - \mathbf{m}_\varrho](z), \Phi^\tau(z) \rangle_z \rho^{\tau, \beta_\tau}(dz) \\ &= \iint \langle \tilde{\nabla}_d^1 k(z, w), \Phi^\tau(z) \rangle_z \rho^{\tau, \beta_\tau}(dz) \rho^\tau(dw) - \iint \langle \tilde{\nabla}_d^1 k(z, w), \Phi^\tau(z) \rangle_z \rho^{\tau, \beta_\tau}(dz) \varrho(dw) \\ &= \frac{1}{2} \iint \langle \tilde{\nabla}_d^1 k(z, w), \Phi^\tau(z) \rangle_z \rho^{\tau, \beta_\tau}(dz) \rho^\tau(dw) + \frac{1}{2} \iint \langle \tilde{\nabla}_d^2 k(z, w), \Phi^\tau(w) \rangle_w \rho^{\tau, \beta_\tau}(dw) \rho^\tau(dz) \\ &\quad - \iint \langle \tilde{\nabla}_d^1 k(z, w), \Phi^\tau(z) \rangle_z \rho^{\tau, \beta_\tau}(dz) \varrho(dw) \\ &= \frac{1}{2} \iiint \langle \tilde{\nabla}_d^1 k(f^{\beta_\tau}(z, u), w), \Phi^\tau(f^{\beta_\tau}(z, u)) \rangle_{f^{\beta_\tau}(z, u)} \rho^\tau(dz) g(du) \rho^\tau(dw) \\ &\quad + \frac{1}{2} \iiint \langle \tilde{\nabla}_d^2 k(z, f^{\beta_\tau}(w, v)), \Phi^\tau(f^{\beta_\tau}(w, v)) \rangle_{f^{\beta_\tau}(w, v)} \rho^\tau(dw) g(dv) \rho^\tau(dz) \\ &\quad - \iiint \langle \tilde{\nabla}_d^1 k(f^{\beta_\tau}(z, u), w), \Phi^\tau(f^{\beta_\tau}(z, u)) \rangle_{f^{\beta_\tau}(z, u)} \rho^\tau(dz) g(du) \varrho(dw), \end{aligned}$$

where the third equality is due to the symmetry of k and relation (3.6). Therefore, it follows that

$$\begin{aligned}
& \mathcal{F}[\rho^{\tau+1}] - \mathcal{F}[\rho^\tau] - s_\tau I \\
&= \frac{1}{2} \iiint \left\{ k\left(h(f^{\beta_\tau}(z, u)), h(f^{\beta_\tau}(w, v))\right) - k(z, w) \right. \\
&\quad \left. - \left[\langle \tilde{\nabla}_d^1 k(f^{\beta_\tau}(z, u), w), s_\tau \Phi^\tau(f^{\beta_\tau}(z, u)) \rangle_{f^{\beta_\tau}(z, u)} \right. \right. \\
&\quad \left. \left. + \langle \tilde{\nabla}_d^2 k(z, f^{\beta_\tau}(w, v)), s_\tau \Phi^\tau(f^{\beta_\tau}(w, v)) \rangle_{f^{\beta_\tau}(w, v)} \right] \right\} \rho^\tau(dz) g(du) \rho^\tau(dw) g(dv) \\
&\quad - \iiint \left\{ k\left(h(f^{\beta_\tau}(z, u)), w\right) - k(z, w) - \langle \tilde{\nabla}_d^1 k(f^{\beta_\tau}(z, u), w), s_\tau \Phi^\tau(f^{\beta_\tau}(z, u)) \rangle_{f^{\beta_\tau}(z, u)} \right\} \\
&\quad \rho^\tau(dz) g(du) \varrho(dw).
\end{aligned}$$

As $h(z) = \exp_z(s_\tau \Phi^\tau(z))$ and $s_\tau \in (0, \varepsilon_0]$, we can now use the Lipschitz-gradient condition (A.11) for k to obtain

$$\begin{aligned}
& \mathcal{F}[\rho^{\tau+1}] - \mathcal{F}[\rho^\tau] - s_\tau I \\
&\leq \frac{L}{2} \iiint \left[\|s_\tau \Phi^\tau(f^{\beta_\tau}(z, u))\|_{f^{\beta_\tau}(z, u)}^2 + \|s_\tau \Phi^\tau(f^{\beta_\tau}(w, v))\|_{f^{\beta_\tau}(w, v)}^2 \right] \rho^\tau(dz) g(du) \rho^\tau(dw) g(dv) \\
&\quad + L \iiint \|s_\tau \Phi^\tau(f^{\beta_\tau}(z, u))\|_{f^{\beta_\tau}(z, u)}^2 \rho^\tau(dz) \varrho(dw) g(du) \\
&= 2Ls_\tau^2 \iint \|\Phi^\tau(f^{\beta_\tau}(z, u))\|_{f^{\beta_\tau}(z, u)}^2 \rho^\tau(dz) g(du).
\end{aligned}$$

Using the definition $\rho^{\tau, \beta_\tau} = f_{\#}^{\beta_\tau}(\rho^\tau \otimes g)$ and the fact $I = -\int_{\mathcal{Z}} \|\Phi^\tau(z)\|_z^2 \rho^{\tau, \beta_\tau}(dz)$, we can rewrite this more compactly as

$$\begin{aligned}
\mathcal{F}[\rho^{\tau+1}] - \mathcal{F}[\rho^\tau] &\leq -s_\tau(1 - 2Ls_\tau) \int_{\mathcal{Z}} \|\Phi^\tau(z)\|_z^2 \rho^{\tau, \beta_\tau}(dz) \\
&= -s_\tau(1 - 2Ls_\tau) \int_{\mathcal{Z}} \|\tilde{\nabla}_d[\mathbf{m}_{\rho^\tau} - \mathbf{m}_\varrho](z)\|_z^2 \rho^{\tau, \beta_\tau}(dz).
\end{aligned}$$

This together with condition (4.4) gives

$$\mathcal{F}[\rho^{\tau+1}] \leq (1 - a_\tau) \mathcal{F}[\rho^\tau] \quad \text{with} \quad a_\tau := \lambda s_\tau (1 - 2Ls_\tau) \beta_\tau^2.$$

In particular, we must have $a_i \leq 1$. By iterating this estimate, we obtain

$$\mathcal{F}[\rho^{\tau+1}] \leq \mathcal{F}[\rho^0] \prod_{i=0}^{\tau} (1 - a_i). \tag{A.15}$$

Due to $1 - x \leq \exp(-x)$ for every number $x \geq 0$, we get $\prod_{i=0}^{\tau} (1 - a_i) \leq \exp(-\sum_{i=0}^{\tau} a_i)$. This together with (A.15) yields the conclusion of the proposition. \square

B Implementation Details And Additional Results

We use $\nabla_{\mathbb{B}}^1 k(x, \mu, \Sigma, w)$ to denote the last component in (3.6) for the gradient $\tilde{\nabla}_d$ of the function $(x, \mu, \Sigma) \mapsto k(x, \mu, \Sigma, w)$. Precisely,

$$\nabla_{\mathbb{B}}^1 k(x, \mu, \Sigma, w) := 2[\nabla_{\Sigma} k(x, \mu, \Sigma, w)]\Sigma + 2\Sigma[\nabla_{\Sigma} k(x, \mu, \Sigma, w)].$$

B.1 Algorithms

Algorithm 2 Discretized Gradient Flow Algorithm for Scheme (4.2) – Detailed Version of Algorithm 1

- 1: **Input:** a source distribution $\rho^0 = \frac{1}{N} \sum_{i=1}^N \delta_{(x_i^0, \mu_i^0, \Sigma_i^0)}$, a sample $\frac{1}{M} \sum_{j=1}^M \delta_{(\bar{x}_j, \bar{\mu}_j, \bar{\Sigma}_j)}$ for the target distribution ϱ , a number T of iterations for training, a sequence of step sizes $s_{\tau} > 0$ with $\tau = 0, 1, \dots, T$, and a kernel k .
 - 2: **Initialization:**
 - 3: Compute $(\bar{\Psi}_1, \bar{\Psi}_2, \bar{\Psi}_3)(x, \mu, \Sigma) = \frac{1}{M} \sum_{j=1}^M (\nabla_x, \nabla_{\mu}, \nabla_{\mathbb{B}}^1)k(x, \mu, \Sigma, \bar{x}_j, \bar{\mu}_j, \bar{\Sigma}_j)$
 - 4: $\tau \leftarrow 0$
 - 5: **while** $\tau < T$ **do**
 - 6: Compute $(\Psi_1^{\tau}, \Psi_2^{\tau}, \Psi_3^{\tau})(x, \mu, \Sigma) = \frac{1}{N} \sum_{i=1}^N (\nabla_x, \nabla_{\mu}, \nabla_{\mathbb{B}}^1)k(x, \mu, \Sigma, x_i^{\tau}, \mu_i^{\tau}, \Sigma_i^{\tau})$
 - 7: **for** $i = 1, \dots, N$ **do**
 - 8: $x_i^{\tau+1} \leftarrow x_i^{\tau} + s_{\tau}(\bar{\Psi}_1 - \Psi_1^{\tau})(x_i^{\tau}, \mu_i^{\tau}, \Sigma_i^{\tau})$
 - 9: $\mu_i^{\tau+1} \leftarrow \mu_i^{\tau} + s_{\tau}(\bar{\Psi}_2 - \Psi_2^{\tau})(x_i^{\tau}, \mu_i^{\tau}, \Sigma_i^{\tau})$
 - 10: $\Sigma_i^{\tau+1} \leftarrow \left(I + s_{\tau} L_{\Sigma_i^{\tau}} [(\bar{\Psi}_3 - \Psi_3^{\tau})(x_i^{\tau}, \mu_i^{\tau}, \Sigma_i^{\tau})] \right) \Sigma_i^{\tau} \left(I + s_{\tau} L_{\Sigma_i^{\tau}} [(\bar{\Psi}_3 - \Psi_3^{\tau})(x_i^{\tau}, \mu_i^{\tau}, \Sigma_i^{\tau})] \right)$
 - 11: **end for**
 - 12: Set $\tau \leftarrow \tau + 1$
 - 13: **end while**
 - 14: **Output:** $\rho^T = \frac{1}{N} \sum_{i=1}^N \delta_{(x_i^T, \mu_i^T, \Sigma_i^T)}$
-

B.2 Kernel and Its Gradient for Implementation

We use the kernel k given by:

$$k((x, \mu, \Sigma), (\bar{x}, \bar{\mu}, \bar{\Sigma})) := \exp(-\alpha \|x - \bar{x}\|_2^2) \exp(-\beta \|\mu - \bar{\mu}\|_2^2) \exp(-\gamma \|\Sigma - \bar{\Sigma}\|_2^2),$$

where α, β and γ are parameters (bandwidth) of the kernel. We note that this kernel is characteristic by [Szabó and Sriperumbudur, 2018, Theorem 4]. Then its standard Euclidean gradient is given by

$$\nabla_{(x, \mu, \Sigma)} k((x, \mu, \Sigma), (\bar{x}, \bar{\mu}, \bar{\Sigma})) = -2 \exp(-\alpha \|x - \bar{x}\|_2^2 - \beta \|\mu - \bar{\mu}\|_2^2 - \gamma \|\Sigma - \bar{\Sigma}\|_2^2) \begin{bmatrix} \alpha(x - \bar{x}) \\ \beta(\mu - \bar{\mu}) \\ \gamma(\Sigma - \bar{\Sigma}) \end{bmatrix}.$$

Thus by plugging into formula (3.6), we obtain

$$\begin{aligned} & \tilde{\nabla}_d^1 k((x, \mu, \Sigma), (\bar{x}, \bar{\mu}, \bar{\Sigma})) \\ &= -2 \exp(-\alpha \|x - \bar{x}\|_2^2 - \beta \|\mu - \bar{\mu}\|_2^2 - \gamma \|\Sigma - \bar{\Sigma}\|_2^2) \begin{bmatrix} \alpha(x - \bar{x}) \\ \beta(\mu - \bar{\mu}) \\ 2\gamma(2\Sigma^2 - \Sigma\bar{\Sigma} - \bar{\Sigma}\Sigma) \end{bmatrix}. \end{aligned}$$

That is,

$$\begin{aligned} \nabla_x k((x, \mu, \Sigma), (\bar{x}, \bar{\mu}, \bar{\Sigma})) &= -2 \exp(-\alpha \|x - \bar{x}\|_2^2 - \beta \|\mu - \bar{\mu}\|_2^2 - \gamma \|\Sigma - \bar{\Sigma}\|_2^2) \alpha(x - \bar{x}), \\ \nabla_{\mu} k((x, \mu, \Sigma), (\bar{x}, \bar{\mu}, \bar{\Sigma})) &= -2 \exp(-\alpha \|x - \bar{x}\|_2^2 - \beta \|\mu - \bar{\mu}\|_2^2 - \gamma \|\Sigma - \bar{\Sigma}\|_2^2) \beta(\mu - \bar{\mu}), \\ \nabla_{\mathbb{B}}^1 k((x, \mu, \Sigma), (\bar{x}, \bar{\mu}, \bar{\Sigma})) &= -2 \exp(-\alpha \|x - \bar{x}\|_2^2 - \beta \|\mu - \bar{\mu}\|_2^2 - \gamma \|\Sigma - \bar{\Sigma}\|_2^2) 2\gamma(2\Sigma^2 - \Sigma\bar{\Sigma} - \bar{\Sigma}\Sigma). \end{aligned}$$

Algorithm 3 Discretized Gradient Flow Algorithm for Scheme (4.3)

- 1: **Input:** a source distribution $\rho^0 = \frac{1}{N} \sum_{i=1}^N \delta_{(x_i, \mu_i, \Sigma_i)}$, a target distribution $\varrho = \frac{1}{M} \sum_{j=1}^M \delta_{(\bar{x}_j, \bar{\mu}_j, \bar{\Sigma}_j)}$, number of iterations T , step sizes $s_\tau > 0$, noise levels β_τ , and a kernel k .
 - 2: **Initialization:**
 - 3: Compute $(\bar{\Psi}_1, \bar{\Psi}_2, \bar{\Psi}_3)(x, \mu, \Sigma) = \frac{1}{M} \sum_{j=1}^M (\nabla_x, \nabla_\mu, \nabla_{\mathbb{B}}^1) k(x, \mu, \Sigma, \bar{x}_j, \bar{\mu}_j, \bar{\Sigma}_j)$
 - 4: $\tau \leftarrow 0$
 - 5: **while** $\tau < T$ **do**
 - 6: Compute $(\Psi_1^\tau, \Psi_2^\tau, \Psi_3^\tau)(x, \mu, \Sigma) = \frac{1}{N} \sum_{j=1}^N (\nabla_x, \nabla_\mu, \nabla_{\mathbb{B}}^1) k(x, \mu, \Sigma, x_j^\tau, \mu_j^\tau, \Sigma_j^\tau)$
 - 7: **for** $i = 1, \dots, N$ **do**
 - 8: Perturb $x_i^{\tau,p} \leftarrow x_i^\tau + \beta_\tau \mathcal{N}_{\mathbb{R}^m}(0, 1)$ and $\mu_i^{\tau,p} \leftarrow \mu_i^\tau + \beta_\tau \mathcal{N}_{\mathbb{R}^n}(0, 1)$
 - 9: Set $S \leftarrow \beta_\tau \mathcal{N}_{\mathbb{S}^n}(0, 1)$ and perturb $\Sigma_i^{\tau,p} \leftarrow (I + \mathbb{L}_{\Sigma_i^\tau}[S]) \Sigma_i^\tau (I + \mathbb{L}_{\Sigma_i^\tau}[S])$
 - 10: $x_i^{\tau+1} \leftarrow x_i^{\tau,p} + s_\tau (\bar{\Psi}_1 - \Psi_1^\tau)(x_i^{\tau,p}, \mu_i^{\tau,p}, \Sigma_i^{\tau,p})$
 - 11: $\mu_i^{\tau+1} \leftarrow \mu_i^{\tau,p} + s_\tau (\bar{\Psi}_2 - \Psi_2^\tau)(x_i^{\tau,p}, \mu_i^{\tau,p}, \Sigma_i^{\tau,p})$
 - 12: $\Sigma_i^{\tau+1} \leftarrow \left((I + s_\tau \mathbb{L}_{\Sigma_i^{\tau,p}} [(\bar{\Psi}_3 - \Psi_3^\tau)(x_i^{\tau,p}, \mu_i^{\tau,p}, \Sigma_i^{\tau,p})]) \Sigma_i^{\tau,p} \left(I + s_\tau \mathbb{L}_{\Sigma_i^{\tau,p}} [(\bar{\Psi}_3 - \Psi_3^\tau)(x_i^{\tau,p}, \mu_i^{\tau,p}, \Sigma_i^{\tau,p})] \right) \right)$
 - 13: **end for**
 - 14: Set $\tau \leftarrow \tau + 1$
 - 15: **end while**
 - 16: **Output:** $\rho^T = \frac{1}{N} \sum_{i=1}^N \delta_{(x_i^T, \mu_i^T, \Sigma_i^T)}$
-

B.3 Label Projection

We here propose an approach to recover new samples in the feature-label space from an empirical distribution in the feature-Gaussian space. Consider that after T iterations of the gradient algorithms, we arrive at a distribution $\rho^T = \frac{1}{N} \sum_{i=1}^N \delta_{(x_i^T, \mu_i^T, \Sigma_i^T)}$. We would like to recover a distribution $\nu^T \in \mathcal{P}(\mathcal{X} \times \mathcal{Y})$ which is induced by ρ^T . As such, we would like to find a distribution ν^T of the form

$$\nu^T = \frac{1}{N} \sum_{i=1}^N \delta_{(x_i^T, y_i^T)}$$

which corresponds to new target samples $(x_i^T, y_i^T)_{i=1}^N$. Moreover, we are interested in recovering labels within the target domain. To this end, let $\mathcal{Y}_{\text{target}} = \{y \in \mathcal{Y} : \exists j \in [M] \text{ such that } \bar{y}_j = y\}$ be the set of labels in the target dataset, and remind that for any $y \in \mathcal{Y}_{\text{target}}$, $(\bar{\mu}_y, \bar{\Sigma}_y) \in \mathbb{R}^n \times \mathbb{S}_+^n$ is the mean vector and the covariance matrix of the distribution of $\phi(X)$ given $Y = y$. Notice that the mean-covariance embeddings $(\bar{\mu}_y, \bar{\Sigma}_y)$ for $y \in \mathcal{Y}_{\text{target}}$ depend only on the target domain data, and it does not depend on the incumbent distribution ρ^T , nor does it depend on the source dataset. Moreover, we can also compute \bar{N}_y as the number of samples from the target dataset with label y .

Because $(\bar{\mu}_y, \bar{\Sigma}_y)$ is readily computed, we can consider $(\bar{\mu}_y, \bar{\Sigma}_y)$ as the centroids and simply find an assignment that minimizes the sum of distances from (μ_i^T, Σ_i^T) to these centroids. We thus can assign each sample from ρ^T to the target labels by solving the linear program

$$\begin{aligned} \min \quad & \sum_{i=1}^N \sum_{y \in \mathcal{Y}_{\text{target}}} \theta_{iy} \sqrt{\|\mu_i^T - \bar{\mu}_y\|_2^2 + \mathbb{B}(\Sigma_i^T, \bar{\Sigma}_y)^2} \\ \text{s.t.} \quad & \sum_{y \in \mathcal{Y}_{\text{target}}} \theta_{iy} = \frac{1}{N} \quad \forall i = 1, \dots, N, \quad \sum_{i=1}^N \theta_{iy} = \frac{\bar{N}_y}{N} \quad \forall y \in \mathcal{Y}_{\text{target}}, \quad \theta \in [0, 1]^{N \times |\mathcal{Y}_{\text{target}}|}, \end{aligned} \tag{B.1}$$

Notice that the assignment problem above does not utilize the information from the covariate x_i^T . Let θ^* be the optimal solution of the above optimization problem. Then the dataset $(x_i^T, z_i^T)_{i=1}^N$ recovered from ρ^T is

$$\nu^T = \frac{1}{N} \sum_{i=1}^N \delta_{(x_i^T, y_i^T)}, \quad y_i^T = \sum_{y \in \mathcal{Y}_{\text{target}}} y \mathbb{1}(\theta_{iy}^* = \max\{\theta_i^*\}) \quad \forall i = 1, \dots, N.$$

We used the POT library to solve the label recovery problem (B.1).

B.4 Results on Mixture of Gaussians

We test our algorithm on a toy example: a mixture of Gaussian distributions to another mixture of Gaussian distributions.

The source distribution and target distribution are:

$$\begin{aligned}
 p_s(x) &= \frac{1}{4} \mathcal{N} \left(\begin{pmatrix} 2.0 \\ -0.3 \end{pmatrix}, \begin{pmatrix} 0.14 & -0.00 \\ -0.00 & 0.22 \end{pmatrix} \right) + \frac{1}{4} \mathcal{N} \left(\begin{pmatrix} 2.0 \\ 0.3 \end{pmatrix}, \begin{pmatrix} 0.43 & 0.18 \\ 0.18 & 0.26 \end{pmatrix} \right) \\
 &+ \frac{1}{4} \mathcal{N} \left(\begin{pmatrix} -0.3 \\ 2.0 \end{pmatrix}, \begin{pmatrix} 0.66 & 0.02 \\ 0.02 & 0.63 \end{pmatrix} \right) + \frac{1}{4} \mathcal{N} \left(\begin{pmatrix} 0.3 \\ -2.0 \end{pmatrix}, \begin{pmatrix} 0.39 & -0.02 \\ -0.02 & 0.13 \end{pmatrix} \right) \\
 p_t(x) &= \frac{1}{4} \mathcal{N} \left(\begin{pmatrix} 2.9 \\ 0.1 \end{pmatrix}, \begin{pmatrix} 0.16 & 0.03 \\ 0.03 & 0.20 \end{pmatrix} \right) + \frac{1}{4} \mathcal{N} \left(\begin{pmatrix} 0.9 \\ 0.5 \end{pmatrix}, \begin{pmatrix} 0.22 & 0.16 \\ 0.16 & 0.46 \end{pmatrix} \right) \\
 &+ \frac{1}{4} \mathcal{N} \left(\begin{pmatrix} 0.8 \\ 2.2 \end{pmatrix}, \begin{pmatrix} 0.63 & 0.02 \\ 0.02 & 0.66 \end{pmatrix} \right) + \frac{1}{4} \mathcal{N} \left(\begin{pmatrix} 1.4 \\ -1.8 \end{pmatrix}, \begin{pmatrix} 0.18 & 0.10 \\ 0.10 & 0.36 \end{pmatrix} \right)
 \end{aligned}$$

From each distribution, we sample 25 particles and flow the particles' positions, means, and covariance simultaneously using Alg. 1. After the algorithm converges, we recover the particles' label in the feature-label space by solving problem (B.1).

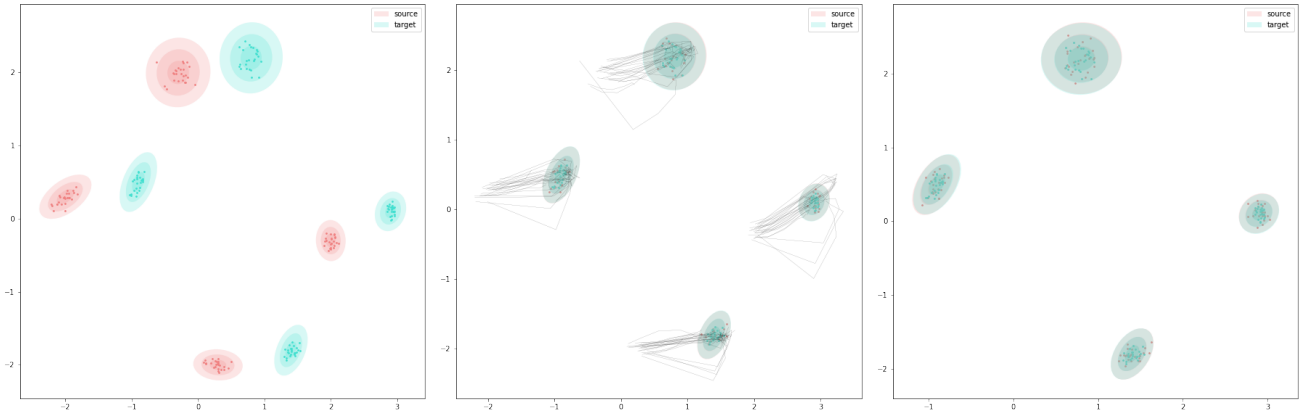


Figure 4: The results of flowing a mixture of 4 Gaussian distributions to a mixture of 4 Gaussian distributions. We demonstrate the initialization (left), the trace of particles in first 200 steps (middle), and the results at step 1000 (right).

We test how our algorithm deals with flowing a mixture of 2 Gaussian distributions to a mixture of 4 Gaussian distributions. From the trace of first 200 steps, we demonstrate that each source Gaussian distribution splits into 2 Gaussian distributions. The source distribution and target distribution are:

$$\begin{aligned}
 p_s(x) &= \frac{1}{2} \mathcal{N} \left(\begin{pmatrix} 0.0 \\ 0.0 \end{pmatrix}, \begin{pmatrix} 0.18 & -0.24 \\ -0.24 & 0.70 \end{pmatrix} \right) + \frac{1}{2} \mathcal{N} \left(\begin{pmatrix} 5.8 \\ 0.0 \end{pmatrix}, \begin{pmatrix} 0.44 & 0.00 \\ 0.00 & 0.87 \end{pmatrix} \right) \\
 p_t(x) &= \frac{1}{4} \mathcal{N} \left(\begin{pmatrix} 2.0 \\ 0.7 \end{pmatrix}, \begin{pmatrix} 0.63 & -0.30 \\ -0.30 & 0.26 \end{pmatrix} \right) + \frac{1}{4} \mathcal{N} \left(\begin{pmatrix} 2.2 \\ -0.8 \end{pmatrix}, \begin{pmatrix} 0.77 & -0.18 \\ -0.18 & 0.55 \end{pmatrix} \right) \\
 &+ \frac{1}{4} \mathcal{N} \left(\begin{pmatrix} 7.0 \\ 0.8 \end{pmatrix}, \begin{pmatrix} 0.63 & -0.30 \\ -0.30 & 0.26 \end{pmatrix} \right) + \frac{1}{4} \mathcal{N} \left(\begin{pmatrix} 7.7 \\ -0.8 \end{pmatrix}, \begin{pmatrix} 0.77 & -0.18 \\ -0.18 & 0.55 \end{pmatrix} \right)
 \end{aligned}$$

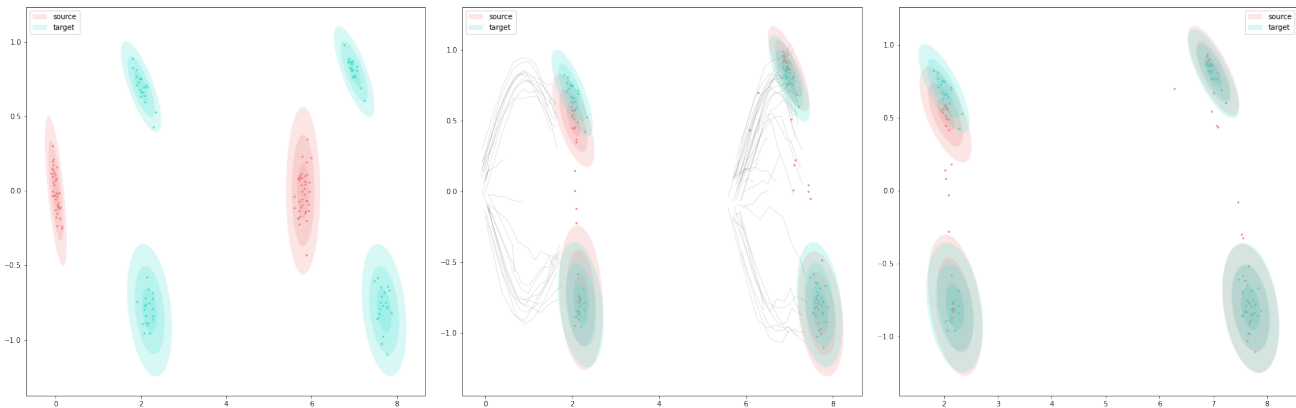


Figure 5: The results of flowing a mixture of 2 Gaussian distributions to a mixture of 4 Gaussian distributions. We demonstrate the initialization (left), the trace of particles in first 200 steps (middle), and the results at step 2400 (right). We use method in Section B.3 to relabel the flowed samples and the labels correspond to their positional belongings correctly.

B.5 Implementation Details

Our algorithms and experiments are implemented in PyTorch. The *NIST images are resized to 20×20 , thus the feature space is of dimension $m = 400$. The SVHN and Tiny ImageNet images are of size $3 \times 64 \times 64$. The classifiers for *NIST datasets are of LeNet-5 architecture. The classifiers for SVHN and Tiny ImageNet are of a ResNet-18 network. For the experiments in Figure 3, we train the classifiers with the set of data 10 epochs with Adam optimizer and learning rate 2×10^{-3} .

When flowing images in *NIST datasets and flowing a mixture of Gaussians, we use the parameters and methods described in Table 2. As we tune the parameters, we notice the algorithm converges with a range of parameters and we report one setting in Table 2.

	SVHN&TIN	*NIST	Gaussian (Figure 4)	Gaussian (Figure 5)
α	0.002	0.001	0.3	0.3
β	0.01	0.002	0.15	0.1
γ	1.0	100	1.0	0.5
initial s_τ	1.0	0.3	0.05	0.03
noise level	0.1	0.01	0	0.1
T	6000	150	2000	2500
Optimizer	RMSprop [Hinton <i>et al.</i> , 2012]	RMSprop	RMSprop	RMSprop

Table 2: Parameters and Optimizer

Our method assumes images of each class form one Gaussian distribution. In reality, the data can be a mixture of Gaussian. To satisfy the Gaussianity assumption, in the preprocessing step, we use a clustering method (k -nearest neighbors) and pick only data from one mode for each class. As a consequence, the data used in the experiment satisfies the conditional Gaussian assumption. For example, the images of the digit 1 can have two modes: slanted left or slanted right. In this case, we can generate two labels (1L, 1R), and the methodology developed in this paper can be applied in a straightforward manner. When testing our transfer learning scheme, we apply the same clustering method on the test dataset, so our test set is within the same mode as our training set.

We store the preprocessed data and apply dimension reduction method on the data’s means and covariance matrices, so the Lyapunov equation is much faster to solve. We use the cluster’s mean and covariance matrix to approximate the 1-shot and 5-shot data’s mean and covariance matrix. In 1-shot learning, the covariance matrix is an identity matrix. All the code and data are available in the supplementary file. We use k -nearest neighbors algorithm to solve the labels of the flowed data, as it performs better with the noisy scheme.

B.6 Additional Results on *NIST Datasets

We conduct additional experiments of flowing between KMNIST and FashionMNIST datasets. The results of our flows are illustrated in the same fashion as Figure 2 and are in the supplementary folder. In each subfigure, each column represents a snapshot of a certain time-step and the samples flow from the source (left) to the target (right). To check if the algorithm is converging, we compute the MMD between the source dataset and the target dataset. Figure 6 is an example of MMD decreasing in transferring the *NIST datasets:

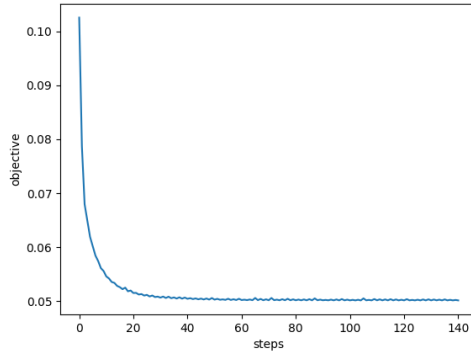


Figure 6: MMD keeps decreasing as we flow the samples from the source domain to the target domain

From FashionMNIST dataset to KMNIST dataset and from KMNIST dataset to FashionMNIST dataset, we also conduct transfer learning experiments. We use the same model architecture and training settings as in Fig. 3. We illustrate the accuracy and error bars of the 1-shot learning and 5-shot learning in Fig. 8. Our flowed samples (S_T) increase the accuracy of the transferred classifiers in both 1-shot and 5-shot learning.

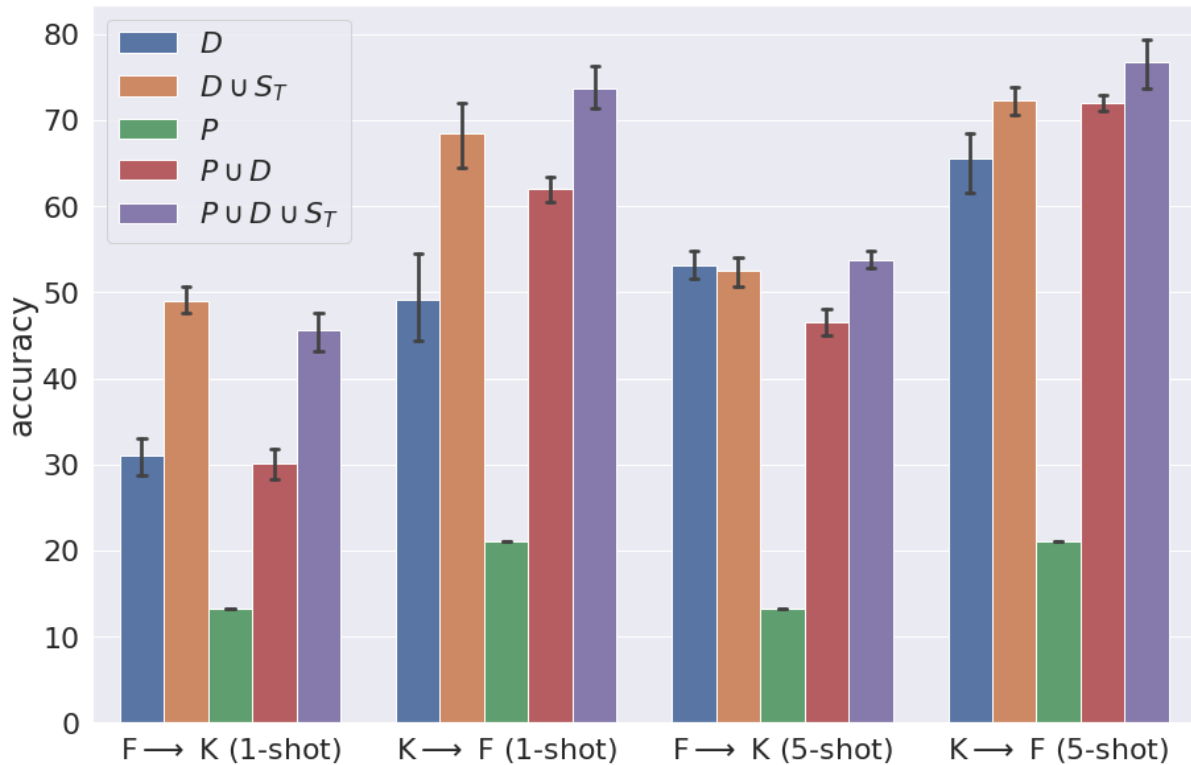


Figure 7: Average target domain accuracy on the test split for transfer learning with one-shot (left) and five-shot (right). Results are taken over 10 independent replications, and the range of accuracy is displayed by the error bars.

B.7 Transfer Learning Results on SVHN and Tiny ImageNet

We run the same transfer learning experiments as section 5.1 on SVHN and Tiny ImageNet datasets and we report the accuracy on the test split³. From the results, we can see S_T always improve the accuracy.

On the higher-dimensional data, it is a lot more difficult to train a strong classifier from only 1 or 5 samples each class, so the accuracy is not so high compared to the *NIST datasets. Another reason is there are only 50 samples in each class of the validation dataset of Tiny ImageNet, so the number of test samples might be too small.

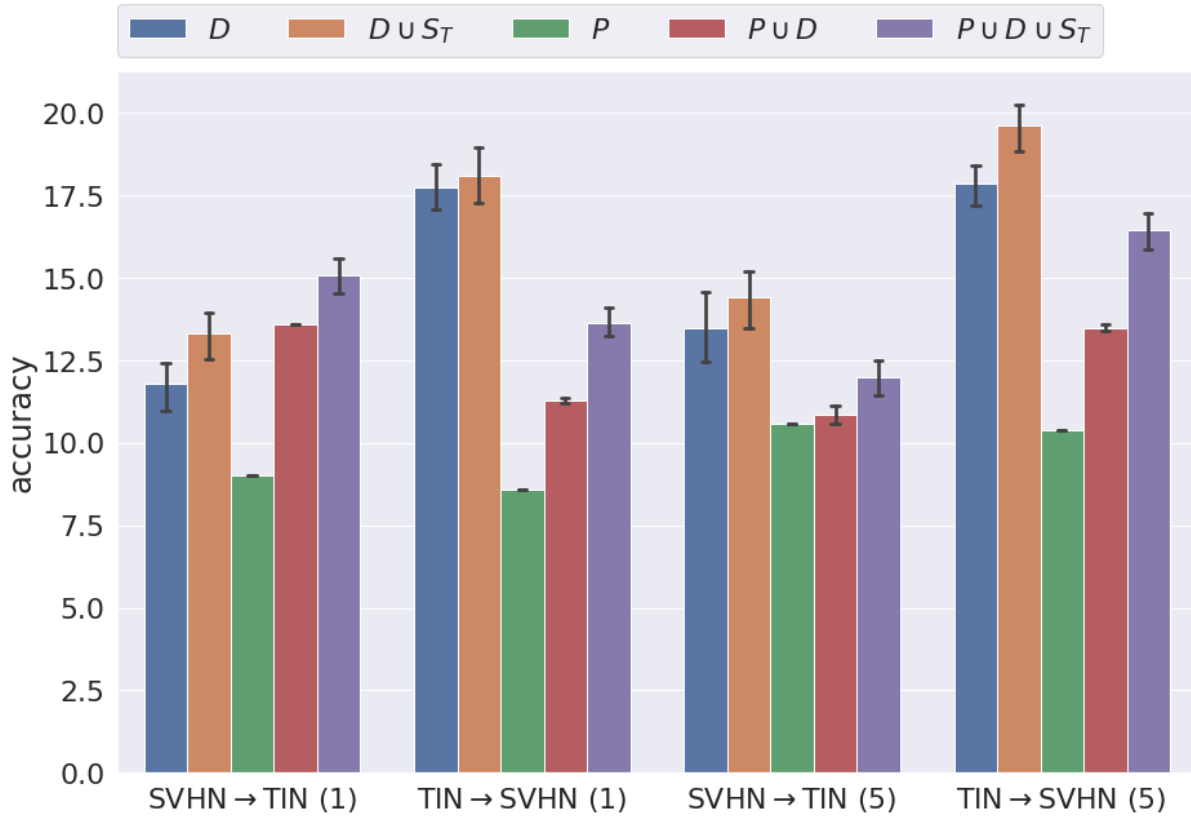


Figure 8: Average target domain accuracy on the test split for transfer learning with one-shot (left) and five-shot (right). Results are taken over 10 independent replications, and the range of accuracy is displayed by the error bars. The 1 and 5 in the parenthesis mean 1-shot and 5-shot transfer learning respectively.

³The Tiny ImageNet dataset does not have labels for the test split, so we use the validation split.

B.8 Comparison with baseline

We compare with [Alvarez-Melis and Fusi, 2021]’s approach as the baseline. We adopted the same values of parameters (number of steps, step size) from the paper of [Alvarez-Melis and Fusi, 2021] and experimented with different values of entropy regularization λ . Entropy regularization λ is a hidden parameter in their code and they reported using the value of $\lambda = 100$ in transfer learning experiments. Also, we experimented with different methods in their code and found that “xyaugm” gives the best qualitative gradient flow results.

We test their algorithm using the same transfer learning setting as ours (using the same clustered data as our experiments), see Table 3 and Table 5 for results. The results show that their method doesn’t improve the classification accuracy after adding the transferred data S_T , if we compare the accuracy $D \cup S_T$ and $P \cup D \cup S_T$ with D and $P \cup D$ correspondingly.

Accuracy	$D \cup S_T$	$P \cup D \cup S_T$
$\lambda = 0.001$	0.1941	0.2478
$\lambda = 0.01$	0.1175	0.2998
$\lambda = 1.0$	0.1739	0.2951
$\lambda = 100$	0.2093	0.3025

Table 3: KMNIST \rightarrow MNIST

Accuracy	$D \cup S_T$	$P \cup D \cup S_T$
$\lambda = 0.001$	0.4488	0.3083
$\lambda = 0.01$	0.3915	0.2897
$\lambda = 1.0$	0.5268	0.4627
$\lambda = 100$	0.2917	0.3307

Table 4: FMNIST \rightarrow MNIST

For runtime comparison, the default device for [Alvarez-Melis and Fusi, 2021]’s code is on the CPU. As we run their code on the GPU, the kernel crashed without giving any informative errors. Thus, we will compare our codes’ runtime per step on the CPU. While our approach takes about 0.512 second, the approach in [Alvarez-Melis and Fusi, 2021] requires 74.78 seconds.

B.9 Comparison with Mixup Method

We run mixup augmentation on $F \rightarrow M$, $K \rightarrow M$, $M \rightarrow F$, and $M \rightarrow K$ on the same one-shot learning setting and same data as ours using the method in [Zhang *et al.*, 2017] with $\alpha = 0.2$ (suggested by [Zhang *et al.*, 2017]). The results are in Table 5. When comparing D with $D \cup S_T$ and $P \cup D$ with $P \cup D \cup S_T$, the added mixup samples (S_T) decrease the accuracy. A reason could be that there are too few examples in the target domain, thus mixup does not add much complexity to the target domain. The mixup experiments in [A] show improvements $< 1\%$, which is much smaller than ours in Fig.3.

Last, we want to emphasize that our gradient flow method aims to increase the number of samples of one distribution, so our method is a complement to augmentation methods. Both gradient flow and augmentation methods are applied in practice at the same time.

Training Data	F→M	K→M	M→F	M→K
D	0.524	0.529	0.506	0.242
$D \cup S_T$	0.488	0.458	0.472	0.141
P	0.097	0.033	0.037	0.089
$P \cup D$	0.510	0.543	0.541	0.140
$P \cup D \cup S_T$	0.467	0.363	0.494	0.120

Table 5: FMNIST \rightarrow MNIST

B.10 Comparison with Traditional Augmentation Methods

We conduct the traditional data augmentation methods, including random rotation and Gaussian noise, on the datasets and compare the classification accuracy with our method. The random rotation is from 0 to 90 degrees. The Gaussian noise is with kernel size (5,9) and standard deviation 0.1 and 5. All the comparison results are in Table 6–9.

Through this experiment, we show that using random rotation to augment the dataset does not improve accuracy much and sometimes even decreases the accuracy in all of the eight transfer learning settings. We note that (D , P , $P \cup D$) are settings without augmentation while ($D \cup S_T$, $P \cup D \cup S_T$) are settings with augmentation. Comparing with the results of our proposed gradient flow approach in Figure 3, augmentation (by random rotation) has much lower performances than ours.

Accuracy	$F \rightarrow M$	$K \rightarrow M$	$M \rightarrow F$	$M \rightarrow K$
D	0.535	0.512	0.483	0.240
$D \cup S_T$	0.542	0.498	0.489	0.164
P	0.097	0.033	0.037	0.089
$P \cup D$	0.510	0.543	0.541	0.140
$P \cup D \cup S_T$	0.551	0.581	0.454	0.124

Table 6: 1-shot learning augmented with random rotation

Accuracy	$F \rightarrow M$	$K \rightarrow M$	$M \rightarrow F$	$M \rightarrow K$
D	0.788	0.837	0.519	0.234
$D \cup S_T$	0.569	0.545	0.490	0.174
P	0.097	0.033	0.037	0.089
$P \cup D$	0.772	0.763	0.581	0.178
$P \cup D \cup S_T$	0.738	0.768	0.593	0.199

Table 7: 5-shot learning augmented with random rotation

Accuracy	$F \rightarrow M$	$K \rightarrow M$	$M \rightarrow F$	$M \rightarrow K$
D	0.524	0.529	0.506	0.242
$D \cup S_T$	0.512	0.494	0.452	0.167
P	0.097	0.033	0.037	0.089
$P \cup D$	0.510	0.543	0.541	0.140
$P \cup D \cup S_T$	0.557	0.590	0.454	0.127

Table 8: 1-shot learning augmented with random Gaussian noise

Accuracy	$F \rightarrow M$	$K \rightarrow M$	$M \rightarrow F$	$M \rightarrow K$
D	0.827	0.824	0.549	0.265
$D \cup S_T$	0.792	0.803	0.734	0.320
P	0.097	0.032	0.037	0.089
$P \cup D$	0.779	0.764	0.581	0.178
$P \cup D \cup S_T$	0.832	0.797	0.729	0.258

Table 9: 5-shot learning augmented with random Gaussian noise

We show that adding Gaussian noise improves the accuracy in some settings, for example, $M \rightarrow F$ and $M \rightarrow K$ in 5-shot, but decreases accuracy in many settings. Our gradient flow method improves the accuracy in all the settings when we compare the accuracy without S_T and with S_T .

Finally, we again note that those simple augmentations, for example (adding Gaussian noise or using random rotation which are designed onto the target dataset) can be used as a **complement** to the gradient flow method, which transfers data from the source dataset to the target dataset.

B.11 Random Gaussian Noise to MNIST

In this section, we conduct an experiment that transfers from random noise vectors to MNIST images. The noise vectors are independently drawn from the normal distribution. Thus, the mean of the noise vectors is a zero vector and the covariance matrix is an identity matrix. From this experiment, we want to show that our method can transfer from any distribution to the target distribution.

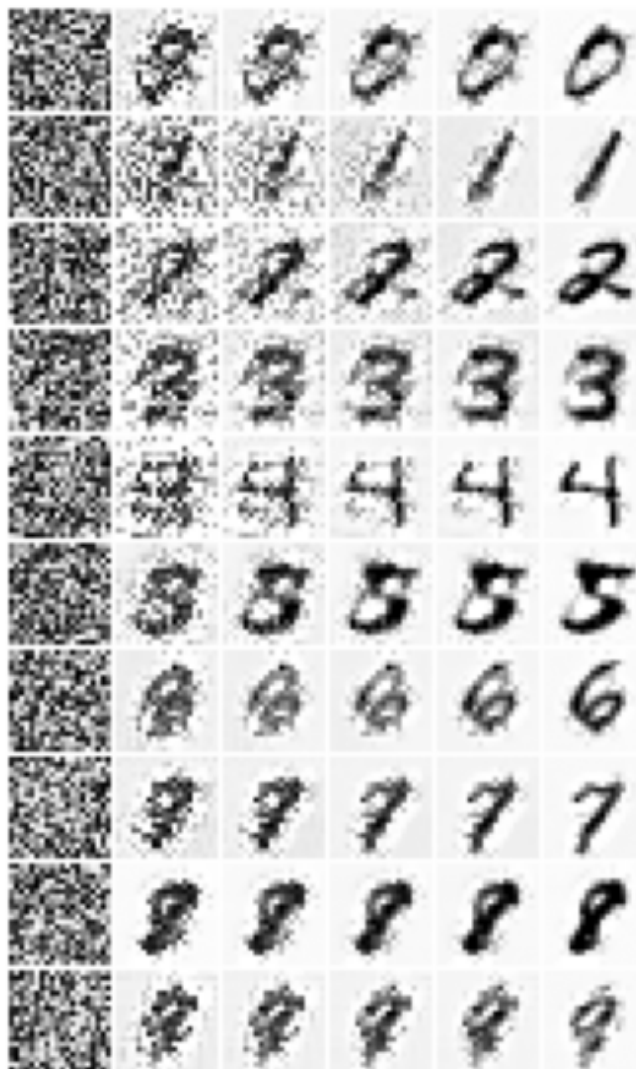


Figure 9: Our method successfully transfers from random noise vectors to MNIST images.

B.12 Evaluation Metric by SSIM and Optimal Transport

We construct a new measure that connects a human perception distance and optimal transport to measure the distance between the distribution of transferred samples and the distribution of target samples.

The target data consists of M samples $(\bar{x}_j, \bar{y}_j)_{j=1}^M$, and the generated data consists of N samples $(x_i^T, y_i^T)_{i=1}^N$. We use the structural similarity index measure (SSIM) [?] to measure image similarity between the generated images and the target images. SSIM measures the similarity between two grayscale images. SSIM is between 0 and 1, and $\text{SSIM} = 1$ means that the two images are identical. Thus, we define a SSIM-based cost to construct a matrix $C \in \mathbb{R}^{N \times M}$: $C_{ij} = 1 - \text{SSIM}(x_i^T, \bar{x}_j)$, for $i = 1, \dots, N$; $j = 1, \dots, M$.

We use the matrix C as a ground transportation cost and solve the Earth Mover Distance problem [?; ?] to obtain the Wasserstein distance between target image and generated image distributions, which are $\frac{1}{N} \sum_{i=1}^N \delta_{(x_i^T, y_i^T)}$ and $\frac{1}{M} \sum_{j=1}^M \delta_{(\bar{x}_j, \bar{y}_j)}$. We compute the distance in 1-shot FashionMNIST to MNIST experiment and Figure 10 plots the distance of each class over 10 independent runs. The plot shows our algorithm successfully decreases the Wasserstein distance between the distribution of generated images and the target distribution during each step.

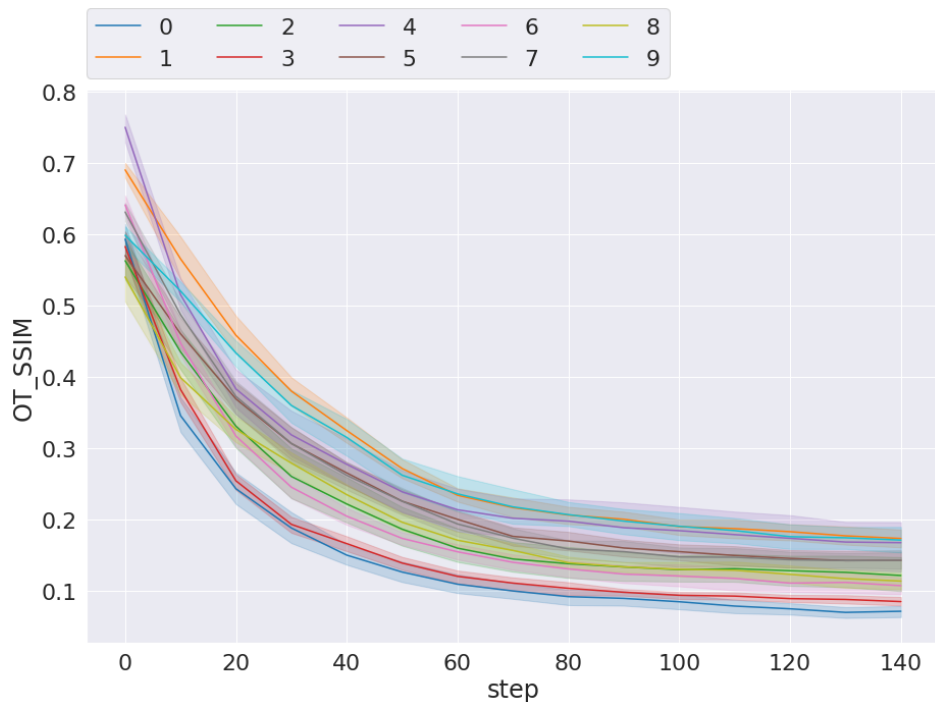


Figure 10: This plots the OT_SSIM distance between the distribution of transferred images and of the target images over 140 steps. The distance decreases as we flow the samples from the source domain to the target domain for every class.